ARMY RESEARCH LABORATORY

Modeling Considerations In The Prediction of Residual Strength In Composite Laminates

Erik Saether

ARL-MR-211

November 1994

DTIC
SELECTED
DEC 2 8 1994
F

"Original contains color plates; All DTIC reproductions will be in black and white"

19941223 056

DTIC QUALITY INSPECTED 1

Approved for public release; distribution unlimited.

The findings in this report are not to be construed as an official Department of the Army position unless so designated by other authorized documents.

Citation of manufacturer's or trade names does not constitute an official endorsement or approval of the use thereof.

Destroy this report when it is no longer needed. Do not return it to the originator.

REPORT DOCUMENTATION PAGE

Form Approved
OMB No. 0704-0188

Public reporting burden for this collection of information is estimated to average 1 hour per response, including the time for reviewing instructions, searching existing data sources, gathering and maintaining the data needed, and completing and reviewing the collection of information. Send comments regarding this burden estimate or any other aspect of this collection of information, including suggestions for reducing this burden, to Washington Headquarters Services, Directorate for Information Operations and Reports, 1215 Jefferson Davis Highway, Suite 1204, Arlington, VA 22202-4302, and to the Office of Management and Budget, Paperwork Reduction Project (0704-0188), Washington, DC 20503.

1. AGENCY USE ONLY *(Leave blank)*	2. REPORT DATE	3. REPORT TYPE AND DATES COVERED
	November 1994	

4. TITLE AND SUBTITLE
Modeling Considerations in the Prediction of Residual Strength in Composite Laminates

5. FUNDING NUMBERS

6. AUTHOR(S)
Eric Saether

7. PERFORMING ORGANIZATION NAME(S) AND ADDRESS(ES)
U.S. Army Research Laboratory
Watertown, MA 02172-0001
ATTN: AMSRL-MA-PC

8. PERFORMING ORGANIZATION REPORT NUMBER
ARL-MR-211

9. SPONSORING/MONITORING AGENCY NAME(S) AND ADDRESS(ES)

10. SPONSORING/MONITORING AGENCY REPORT NUMBER

11. SUPPLEMENTARY NOTES

12a. DISTRIBUTION/AVAILABILITY STATEMENT
Approved for public release; distribution unlimited.

12b. DISTRIBUTION CODE

13. ABSTRACT *(Maximum 200 words)*

The prediction of residual strength in damaged composite structures is complicated by the need to accurately characterize internal damage states and to mathematically simulate the material behavior which displays a variety of damage mechanisms and failure modes. Numerous analyses have been developed which, in general, have been restricted to specific damage modes and idealized geometric configurations. Modeling issues include micromechanical fiber/matrix failure phenomena, delamination growth, buckling of laminate sublayers and nonlinear material and geometric response to applied loads. For the reliable design of composite components, the modeling approaches utilized in various specialized analyses need to be synthesized into a combined, robust methodology. The purpose of the present investigation is to identify the various salient failure phenomena involved in damaged composite laminates and to discuss mathematical modeling approaches to represent such damage. The identification of analytic approaches provide a basis for further extension to overcome existing limitations in the prediction of residual strength.

14. SUBJECT TERMS	15. NUMBER OF PAGES
Composite Laminates, (Math) Modeling, Failure Phenomenon, Residual Strength	52
	16. PRICE CODE

17. SECURITY CLASSIFICATION OF REPORT	18. SECURITY CLASSIFICATION OF THIS PAGE	19. SECURITY CLASSIFICATION OF ABSTRACT	20. LIMITATION OF ABSTRACT
Unclassified	Unclassified	Unclassified	UL

Contents

Codes
Dist
A-1

Contents (cont.)

Figures

Page

Figures

Introduction

In the application of composite materials to structural design, the accurate prediction of residual strength is of prime interest to design engineers to ensure that the material efficiency afforded by composites meet service load conditions while demonstrating survivability and damage tolerance to projected damage-causing threats in the intended service environment. While providing more efficient structures, composites are inherently more complex material systems than metallics and require more elaborate mathematical models to simulate their behavior. The mathematical representation of composite structures is complicated by the dimensional scale at which various phenomena are modeled. Three modeling domains may be loosely defined as the microscopic, lamina and component level. At a microscopic level of analysis, the micromechanical consideration of fiber and matrix characteristics are predominant. These include fiber waviness and weave type, defects such as fiber/matrix debonding, fiber breakage, matrix cracking, porosity and interactive fracture phenomena. It is within this regime that material failure criteria are developed from the analysis of micromechanical damage modes. At the lamina level of consideration, the assumption of a continuum may be applied to represent a composite lamina as a continuous homogeneous material with associated material property tensors defining basic elastic stress/strain relations derived from engineering mixture relations of the bulk properties of the constituent fiber and matrix materials. Ply thickness variations, failure criteria, material damage laws, debonding and delamination growth between adjacent laminae and material nonlinearity lead to mathematical representations that model the progression of damage and failure of individual plies. At the highest level of representation, the mathematical modeling of a composite component generally must account for complex geometries, applied loading and support conditions. Laminate properties may be represented by a summation of averaged ply properties and assumed as continuous throughout the local material domain. Depending on the geometric complexity of the problem being studied, various approaches may be used to model the problem. Mathematical modeling may utilize exact formulations based on elasticity theory, structural engineering approximations such as beam, plate and shell assemblages, or numerical approaches such as finite difference or finite element theory. Regardless of the modeling approach, the global response of the component to applied loading is sought. This response includes the basic displacement and internal stress distribution from which local material failure modes and ply instabilities may be predicted. The analytical prediction of residual strength ranges over three basic scale regimes, each of which requires different modeling considerations.

A myriad of analytical and numerical approaches for predicting residual strength in composites have been formulated by various researchers. These analyses have, in general, been restricted to selected damage modes and to idealized geometric configurations. An overview of selected analyses include those based on fracture mechanics, structural engineering approximations and finite element theory. Reference [1] presents a fracture mechanics approach in which the observed impact damage zone is replaced by an elliptical edge crack. In this model it is assumed that the crack grows laterally across the specimen width without increasing in depth. Under increasing load, shearing at the base of the crack effectively separates or isolates this layer from the rest of the laminate and precipitates ultimate tensile failure. Similar approaches have been applied in which damage due to impact is approximated as through-thickness holes, cracks or inclusions [2-5]. Failure of laminates due to applied in-plane compressive loading have been studied assuming delamination growth and buckling failure as the primary failure modes. Reference [6] considers a multi-beam model to represent delaminations and assesses the effects of support conditions, planarity assumptions of beam rotation and post-buckled behavior on total load carrying capability. Reference [7] adopts a beam

model to assess delamination growth, stability and arrest in a 1-D model of laminate failure. The effect of bridging due to transverse normal stitching on delamination growth is presented in Reference [8]. The study of delamination in a homogeneous, axially loaded plate is presented in Reference [9] in which the effect of delamination position, size, thickness and assumed boundary conditions on critical buckling loads are considered. The effect of an elliptical delamination in a quasi-isotropic composite plate is studied in Reference [10]. The delamination is assumed to be near-surface and a Rayleigh-Ritz approach used to assess the effect of delamination shape, orientation and layup on critical buckling strains. A study of stability in random, short-fiber composite plates is presented in References [11, 12] which also employ a Rayleigh-Ritz analysis and assess delamination growth and coupled local/global buckling phenomena. General studies on delamination stability such as [13, 14] demonstrate that delamination growth can preceed sublaminate buckling. Finite element analysis of residual strength in laminates based on assumed progressive in-plane material failure have been formulated utilizing specialized ply damage laws. Bolted composite joints are analyzed in Reference [15] assessing tension and shear-out failure modes. Reference [16] considers a pin-loaded hole in relation to in-plane material failure modes. Laminated composites containing stress concentration due to a circular cut-out is analyzed in Reference [17]. In the above analyses of in-plane failure, unique material damage laws are developed which differentiate between fiber and matrix modes and includes nonlinear shear stress behavior. The residual tensile strength of impacted laminates is predicted using a ply-level analytical formulation in [18]. The developed analysis avoids plate assumptions of plane stress and utilizes a fully 3-D finite element representation of the laminate. Damage modes are limited to delaminations and fiber breakage which are represented as a through-thickness line crack. A progressive failure analysis is presented in Reference [19] in which the layerwise laminate theory of [20] is used to model the laminate continuum. This analysis improves upon other progressive failure analyses such as those presented in References [21-24] by including failure through delamination. The Tsai-Wu failure criteria is used to predict ply failure and a stiffness reduction model is used to approximate post failure ply behavior. Axial tensile loading is assumed and, in comparison to other structural engineering approximations, it is concluded that a fully 3-dimensional analysis is required for accurate failure prediction.

The purpose of the present investigation is to identify the various failure phenomena involved in damaged composite laminates and to discuss mathematical modeling approaches that have been developed to represent such phenomena. It must be emphasized that research into composite materials has given rise to an extensive literature on composite behavior. The present effort is limited to providing a representational survey of various topics and is constrained to a selective set of analytical developments with which to broadly outline the prediction of residual strength in composites structures. When possible, extensions to overcome limitations in existing analyses are suggested.

The following sections discuss modeling considerations which include a brief description of nondestructive evaluation techniques (NDE) currently used in determining initial damage states, characteristics of composite laminae and laminate response to applied loads. Finally, details of a proposed numerical finite element–based approach are presented in which all important damage modes and their interaction may be accounted for through appropriate solution algorithms. Such an approach is deemed capable of incorporating all relevant phenomena in a predictive methodology to accurately determine the ultimate strength of composite materials in arbitrary structural geometries under general loading and support conditions.

Nondestructive Damage Characterization

Regardless of how accurate any developed analytic methodology is in representing a damaged composite laminate, the prediction of residual strength is entirely dependent on the accuracy of the input defining the internal damage. This accuracy is, in turn, dependent on the capability of existing inspection techniques to resolve internal damage and distinguish different damage modes.

Inspection procedures may be destructive or nondestructive in nature. Destructive characterization, in which a damaged laminate is physically sectioned and microscopically inspected, is useful in providing a quantified assessment of laminate damage type and location due to specific impact events, environmental effects or manufacturing defects. Such an examination, however, precludes subsequent experimental testing of the actual specimen in measuring residual load–carrying capability and a post-failure examination of failure modes. Nondestructive evaluation (NDE) techniques provide detailed information of initial defects and internal damage while allowing subsequent experimental assessment of residual strength. This information used in mathematical simulation of residual strength make possible accept/reject decisions during fabrication or the assessment of repair/no-repair options for composite components effected in service applications.

Several survey articles of current state-of-the-art NDE techniques may be found in References [25-28]. The aim of these techniques is to obtain information or 'signatures' of internal structural features which are used to locate and differentiate various defects and damage. Such internal features include manufacturing defects such as voids, porosity, cracks and ply debonding, service environmental effects such as corrosion and moisture levels, and damage due to overloads or impacts.

Of the multitude of NDE techniques available as mature technologies, a brief outline of several versatile methods are outlined below to give an indication of current capabilities in characterizing internal damage. The selected techniques which are currently in wide use are acoustics/ultrasonics, thermography and radiography.

Acoustics/Ultrasonics

Within this class of techniques, sound or pressure pulses are used to obtain information on internal damage [29-35]. One technique utilizes the acoustical emissions recorded during experimental testing at the onset of component failure to correlate sound frequencies with specific failure modes such as delaminations, matrix cracking and fiber breakage. The simplest use of acoustical emissions is the Tap Test in which a rigid object is lightly tapped along the outer surface. The change in sound pitch of the vibrating laminate can indicate the presence of near surface damage, predominantly delaminations. Ultrasonic inspection techniques utilize a transducer to introduce pressure pulses into the material. The governing equations used to model waves in an isotropic solid are given by

$$\begin{aligned} \rho\frac{\delta^2 u}{\delta t^2} &= (\lambda+2\mu)\frac{\delta^2 u}{\delta x^2}+\mu\frac{\delta^2 u}{\delta y^2}+(\lambda+2\mu)\frac{\delta^2 v}{\delta x\delta y} \\ \rho\frac{\delta^2 v}{\delta t^2} &= (\lambda+2\mu)\frac{\delta^2 v}{\delta x^2}+\mu\frac{\delta^2 u}{\delta y^2}+(\lambda+2\mu)\frac{\delta^2 u}{\delta x\delta y} \end{aligned} \qquad (1)$$

where u and v are the displacements in the x and y directions, t is time, λ and μ are the Lamé constants, and ρ is the density. Internal damage will interact and scatter the stress waves which are recorded as backscatter or through–transmission changes in the input signal. This technique can detect defects and damage modes such as voids and regions of material porosity in addition to delaminations, regions of matrix cracking and fiber breakage. The resolution of damage diminishes with increasing specimen thickness, attenuating features inherent to the material and an increasing number of damage sites along the direction of the wavefront. An example of ultrasonic imaging is presented in Figure 1 showing the profile of square metallic shim positioned at the midplane of a 1" thick S-2 Epoxy woven laminate. The figure demonstrates the capability of imaging a deeply imbedded defect in a woven cloth laminate which presents significant attenuation of induced pressure pulses due to the complex fiber arrangement in the individual ply weaves.

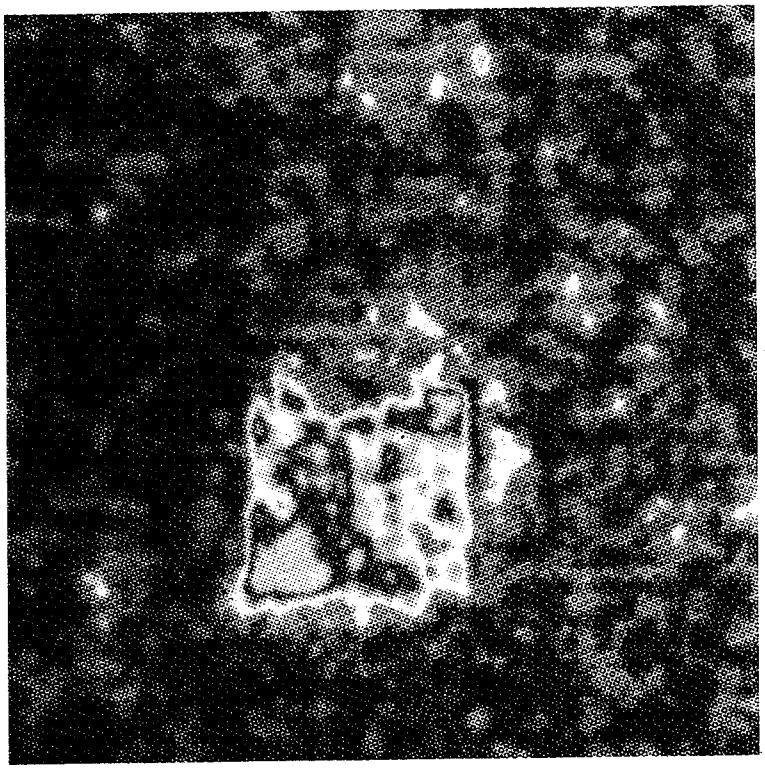

Figure 1. Ultrasonic image of a thick composite panel with simulated damage.

Thermography

Thermal imaging of internal damage is based on the change of temperature distribution in a material. A common form of thermography utilizes the change in thermal conductivity due to material discontinuities associated with different damage states [36,37]. The governing equation may be given by

$$c\rho\frac{\delta T}{\delta t} = \frac{\delta}{\delta x}(k_x\frac{\delta T}{\delta x}) + \frac{\delta}{\delta y}(k_y\frac{\delta T}{\delta y}) + \frac{\delta}{\delta z}(k_z\frac{\delta T}{\delta z}) \tag{2}$$

where T is the temperature, ρ, c and k are the density, specific heat and thermal conductivity, respectively. In applying the technique, thermal energy is introduced into the specimen and infrared thermal emissions are measured to construct images of regions of nonuniform heat flow thus profiling the damage. Thermal gradients may be measured on the same or opposite side of applied heating. Image resolution declines rapidly with increasing depth of internal damage. Alternatively, thermograms may be generated by imaging the internal temperature changes caused by applied loading. A fundamental relationship exists relating internal stresses to generated temperature distributions which are quantified through the equation of state of the material being studied. This phenomenon is formalized in the mathematical theory of thermoelasticity. For an isotropic material, the thermoelastic equilibrium equations relating stresses and temperature are given by

$$\begin{aligned}
\frac{\delta\sigma_{xx}}{\delta x} + \frac{\delta\tau_{xy}}{\delta y} + \frac{\delta\tau_{xz}}{\delta z} &= \frac{\alpha E}{1-2\nu}\frac{\delta T}{\delta x} \\
\frac{\delta\tau_{xy}}{\delta x} + \frac{\delta\sigma_{yy}}{\delta y} + \frac{\delta\tau_{yz}}{\delta z} &= \frac{\alpha E}{1-2\nu}\frac{\delta T}{\delta y} \\
\frac{\delta\tau_{xz}}{\delta x} + \frac{\delta\tau_{yz}}{\delta y} + \frac{\delta\sigma_{zz}}{\delta z} &= \frac{\alpha E}{1-2\nu}\frac{\delta T}{\delta z}
\end{aligned} \tag{3}$$

where E is the Young's modulus, ν is the Poissons ratio and α is the coefficient of thermal expansion. Current sensors can detect temperature changes on the order of $0.001°C$ which gives a resolution comparable to common strain gauges. As stated in Reference [25], refinements in thermographic imaging may be expected through the development of more sensitive signal analysis tools. An example of thermographic imaging is presented in Figure 2 showing the combined stress profile around a 1/4" diameter open hole in a unidirectional Aramid fiber laminate under uniform applied tensile loading.

Figure 2. Thermograph of stresses around an open hole in a loaded specimen.

Radiography

Radiography is a powerful technique for characterizing internal damage in composites [38, 39, 40]. A common form of this technique utilizes high energy electromagnetic radiation in the form of x-rays to measure the changes in absorption due to variations in density. Radiography is an extremely sensitive technique and yields high resolution images of internal damage. Current resolutions obtainable are on the order of 0.1% changes in density. The resulting 2-D damage profiles may be further refined using various image enhancement techniques. In Computed Tomography (CT), 1-D radiographic measurements are made along rays through the specimen at a large number of points around the perimeter. Mathematical image reconstruction algorithms are then utilized to generate a 2-D image of damage in the plane. This may be repeated through the thickness of the specimen to obtain a fully 3-D image of internal damage. This capability coupled with the high sensitivity and resolution of radiography provides a valuable tool for determining the 3-D distribution of various composite damage modes.

Using basic NDE technologies such as those mentioned above to obtain information of internal damage, various image processing algorithms are available for extracting information and characterizing damage [41-44]. Reference [45] explores the post-processing of reconstructed images from computed tomography to identify the 3-D distribution of internal delaminations, fiber and matrix damage regions through modal separation. Images were obtained from thick S-2 Glass composite panels ballistically impacted in a study presented in Reference [46]. Figure 3 shows a representative CT image of impact induced damage at a particular depth level. Research has focused on automatically interpreting the damage signature present in the image to differentiate various damage modes. Figure 4 shows a histogram of pixel intensities which exhibits various clusters of normally distributed intensity levels. These local distributions or modal patterns are logically conjectured to represent separate damage modes and automated algorithms are being developed to interpret these damage signatures.

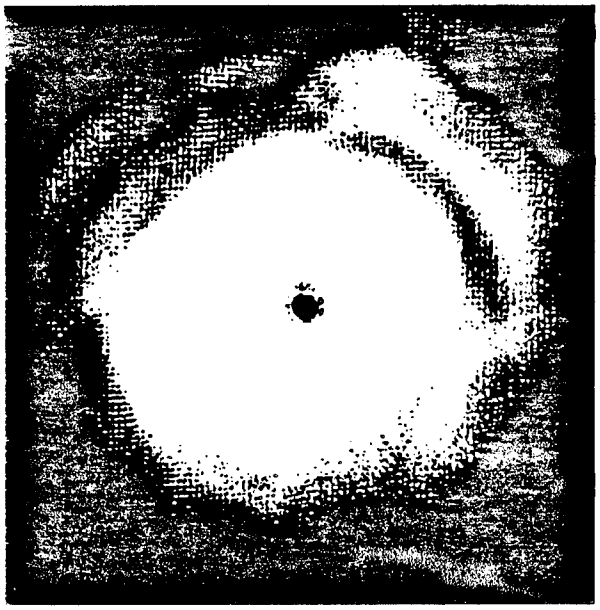

Figure 3. CT image of damage in a composite laminate.

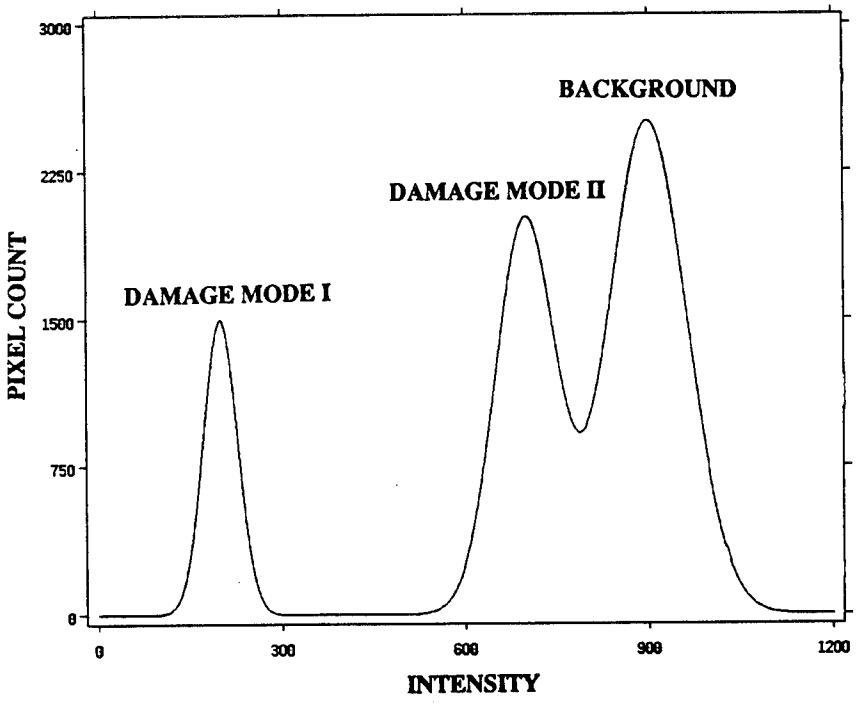

Figure 4. Histogram of image intensities showing damage modes.

The objective of the image analysis is to extract maximum information about the internal damage state which is of paramount importance as input to any developed residual strength prediction methodology.

Characteristics of Composite Laminae

In the mathematical representation of a composite component, the primary constituents of a laminate are the plies or laminae. A lamina consists of an aggregate of high strength fibers embedded in a surrounding polymeric organic matrix. Plies may be formed with long continuous fibers aligned in a principle direction to constitute a tape, with short, randomly oriented fibers forming a transversely isotropic layer, or with fibers arranged in a multitude of different weave patterns constituting a woven cloth ply. This biphasic material system is characterized by fiber orientation, distribution and material properties, matrix material properties and numerous micromechanical aspects including initial manufacturing defects and service load induced damage.

In the development of a residual strength prediction methodology, several aspects of composite laminae are of critical importance in the development of accurate models which include the mathematical representation of a ply as a homogeneous continuum, nonlinear material properties, failure theories, ply strengths and damage laws. These issues are discussed in the following sections.

Continuum Representation

A fundamental aspect in the mathematical representation of laminated composites is the treatment of the ply. The density and distribution of fibers in a ply is altered during curing by the flow of resin and may be described statistically. Fiber volume and the nature of the fiber bonding with the surrounding matrix is important in approximating the gross behavior of the laminae [47]. The modeling of plies or laminae involve micromechanical considerations of fiber continuity, waviness, bonding characteristics with the surrounding matrix, the effect of broken fibers on local stress redistribution and fracture phenomenon dealing with the propagation and interaction of fracture surfaces. For the purpose of macroscopic analysis, these effects are modeled using a continuum assumption in which the lamina elastic properties are determined from a simple mixture rule and the bulk material properties of the fiber and matrix. Micromechanical defects such as fiber-matrix debonding, fiber breakage, matrix cracking, voids, porosity, moisture and temperature effects are represented through appropriate changes to the primary variables - moduli - describing the elastic continuum. These micromechanical bases for macroscopic behavior may be determined analytically by assuming a representative unit cell or volume element which consists of an idealized arrangement of fibers in a surrounding matrix and incorporates assumed micromechanical damage modes. This unit cell is assumed as a fundamental description of the ply continuum and elasticity theory is used to determine the elastic behavior of this fundamental ply unit. An example of a typical two–dimensional unit cell is depicted in Figure 5 showing idealized distributions of broken fibers with regions of fiber/matrix debonding. The results of the stress and failure analysis of the unit cell are scaled up to approximate macroscopic ply behavior.

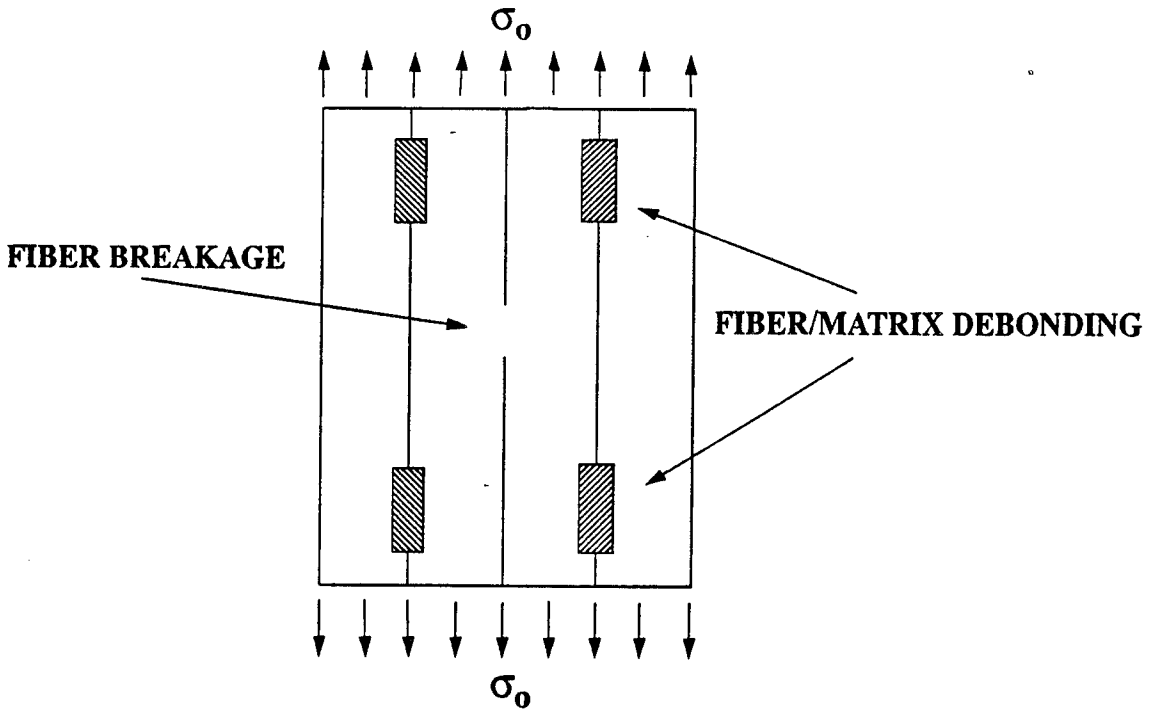

Figure 5. Typical unit cell representation of ply continuum in micromechanical analysis.

The idealization of a ply as an elastic continuum inevitably contributes to the disparity between analytical predictions and actual laminate behavior. The basis for this disparity is inherent to the assumption of homogeneity in a typical ply and may be contrasted with the actual discontinuous and heterogenous ply composition as depicted in Figure 6 which shows a photomicrograph from Reference [48] of a ply with a central vertical crack.

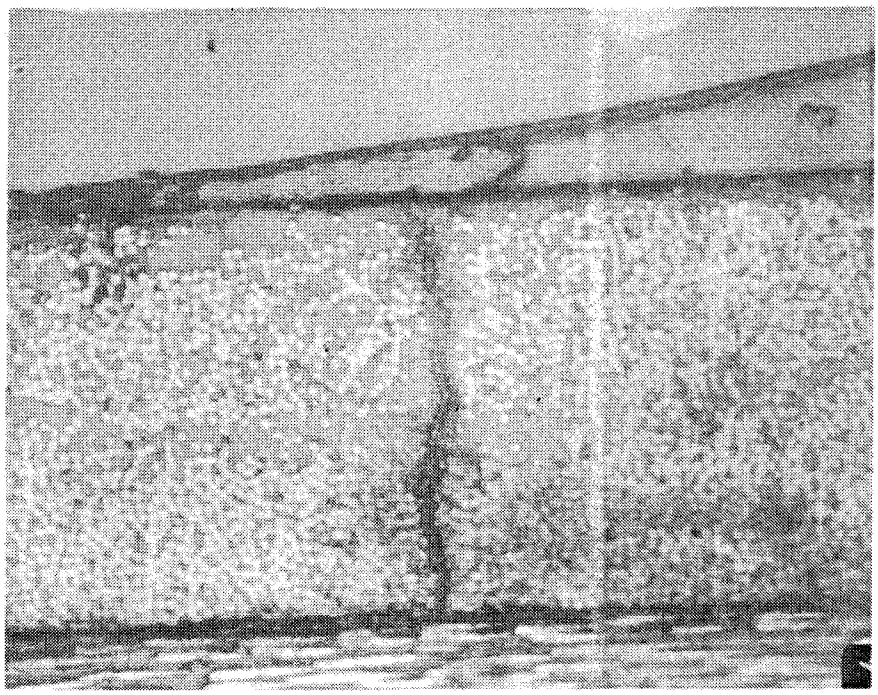

Figure 6. Photomicrograph of a typical ply with a vertical crack.

The complexity of the underlying material composition of individual plies makes the mathematical treatment approximate or statistical in nature. Thus, significant modeling assumptions are present in the basic representation of composite laminae which introduce an inaccuracy and variability to any prediction of composite behavior.

Nonlinear Ply Properties

Few materials maintain a linear elastic or Hookian response to failure, yet the nonlinearities exhibited near the point of failure for many materials are negligible. For composite materials, nonlinear viscoelastic and plastic behavior is commonly neglected and most elastic components may be represented as Hookian or exhibiting a weak nonlinear elastic reponse. Typical fibers used in composite material systems are high strength yet brittle and exhibit a linear stress–strain relation. Matrix materials are usually compliant and exhibit various degress of nonlinear response in high stress regimes. As depicted in Figure 7, the combined effect on lamina behavior is commonly linear with increasing stress until fiber failures begin. In addition, lamina failure strain is typically close to the fiber failure strain.

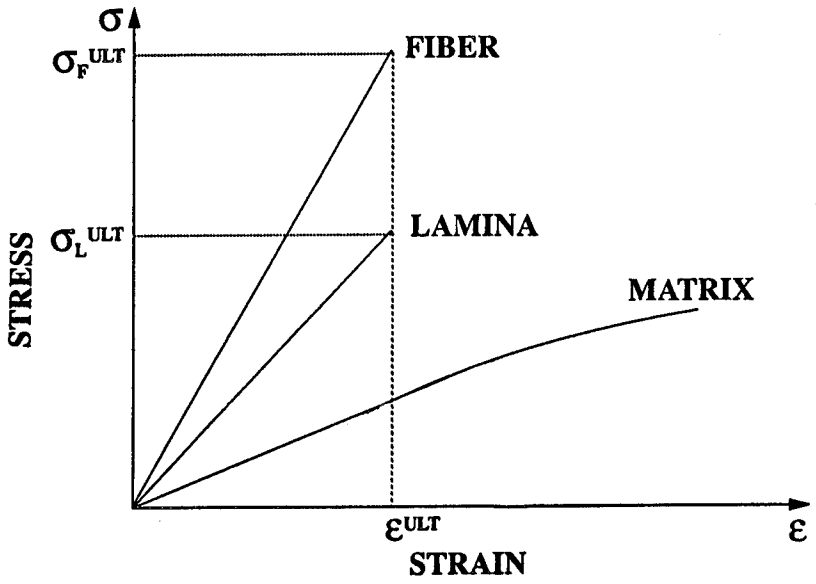

Figure 7. Stress–strain behavior of ply constituents.

For weakly nonlinear ply elastic components, an approximation to the nonlinearities may be made through a bilinear stress-strain relation as shown in Figure 8. The use of a bilinear relationship greatly simplifies analytic formulations over higher-order functional representations.

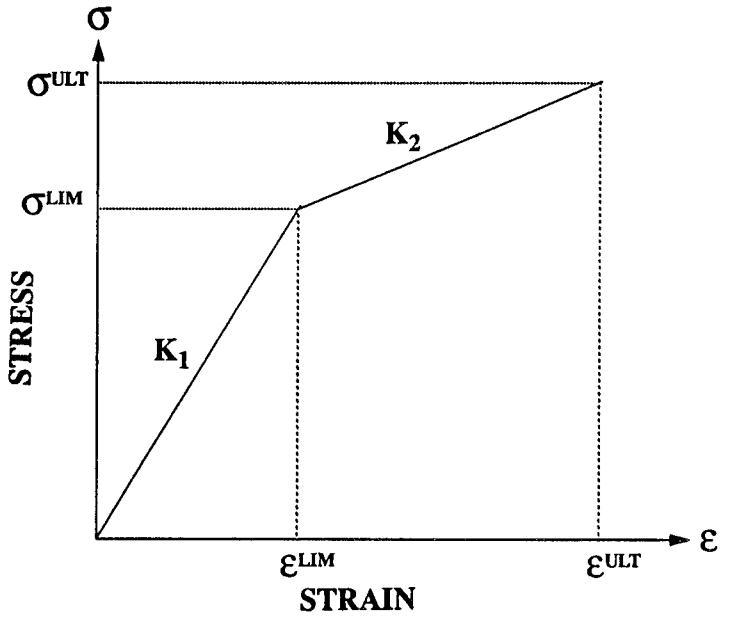

Figure 8. Bilinear stress-strain law.

Certain composite material systems can exhibit significant nonlinear behavior in all or specific elastic moduli. Experimental verification of unidirectional nonlinear ply response under tensile loading is presented in Reference [49]. A gross measure of nonlinearity is presented in the form of an empirical relationship between an averaged Young's modulus and stress level given by

$$E = E_o + 21\sigma \tag{4}$$

For the laminate considered, the increase in Young's modulus from the initial zero stress state to ultimate tensile strength was on the order of 30%. Composite laminates exhibit a significant nonlinearity primarily in the elastic response in the shear modulus [90]. As detailed in Reference [51], a piece-wise linear approximation is given by

$$(G_{12})_n = \frac{(\Delta\tau_{12})_n}{(\Delta\gamma_{12})_n} \tag{5}$$

where at the n^{th} segment along the shear stress/strain curve, the relationship between $\Delta\tau_{12}$ and $\Delta\gamma_{12}$ is given as a function of material compliance and reduced stiffness terms.
A representation developed in [90, 81] for the shear modulus is given by

$$\gamma_{12} = (\frac{1}{G_{12}}) + \alpha(\tau_{12})^3 \tag{6}$$

where G_{12} is the inital shear modulus and α is an experimentally determined constant. The tangent shear modulus at any position on the shear stress-strain curve is given by

$$\bar{\gamma}_{12} = \frac{\delta\tau_{12}}{\delta\gamma_{12}} = (\frac{1}{G_{12}}) + 3\alpha(\tau_{12})^2 \tag{7}$$

It has been noted in [17, 16, 51, 52] that the nonlinearity does not become significant until the ply shear stresses become comparable to the longitudinal tensile stresses. In an analytical methodology, the nonlinear expression may be used in an iterative solution algorithm for predicting laminate response with increasing load. To avoid the computational expense of a nonlinear solution scheme, the shear modulus may be taken as the initial modulus, a median tangent modulus, or, frequently, as a linear approximation using a secant modulus defined by the shear strength and ultimate shear strain. The various definitions of the shear modulus are depicted in Figure 9.

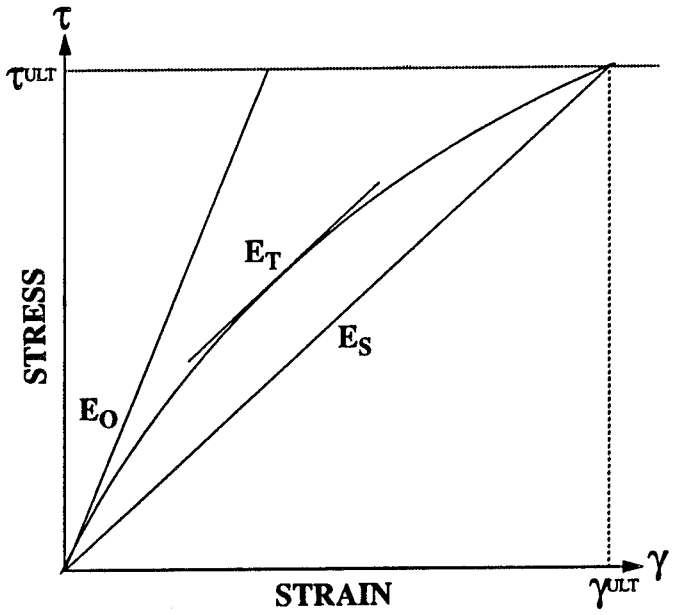

Figure 9. Initial, local tangent and secant shear modulus.

Depending on the laminate ply layup and magnitude of the shear stress, the various approximations in linear analysis may be unacceptably inaccurate in predicting through-thickness stress distribution and, hence, in predicting ply level damage.

Ply Failure Criteria

A primary consideration in the analysis of composite structures is the accurate prediction of ply failure due to a specific state of stress. The complexity of the biphasic ply material makes the analysis of local failure difficult. Under applied external loading, the local stress flow yields a large

number of identifiable failure interactions and damage modes, any one of which can become a critical 'weak–link' in the prediction of ply failure. The difficulty in this endeavor is aptly expressed by a passage from [53]: "The microstructural aspects of failure are of such complexity that there is little hope of resolution of this problem on the basis of micromechanics methods. Such methods would require analytical detection of successive microfailures in terms of microstress analysis and microfailure criteria and prediction of the coalescence of some of them to form macrofailures which is an intractable task." To make the mathematical modeling of such phenomena tractable, simplifying assumptions are made utilizing a fracture mechanics or continuum approach. In a fracture mechanics framework, failure of a ply is based on the predicted growth of initial cracks. A continuum approach assumes that, mathematically, accurate failure criteria involving homogeneous elastic constants exist at a macroscopic level. Material failure mechanisms have been well established for isotropic materials in which different definitions for failure are used such as ultimate strength, yielding, proportional limit, endurance limit and maximum working stress. Numerous failure theories have been advanced by Rankine, Tresca-Guest, St. Venant, Beltrami, Huber–Von Mises–Hencky, and Mohr [54]. These theories are regarded as single-parameter criteria as they are based on a single measure of failure, usually the yield stress of the material. These criteria are, however, inadequate to represent the failure of more complex materials in which strength differs in tension and compression and stress interaction effects are significant. Subsequent failure criteria have been developed for anisotropic materials from simple criteria such as maximum stress/strain to those of Hill [55], Tsai-Hill [56], Hoffman [57] and Tsai-Wu [58] which are referred to as quadratic polynomial theories [59, 60, 61]. Each may be deduced from the general tensor polynomial criteria given by

$$FI = F_i\sigma_i + F_{ij}\sigma_i\sigma_j + F_{ijk}\sigma_i\sigma_j\sigma_k + ... \tag{8}$$

where σ_i are stress tensor components in principle material directions and F_i, F_{ij}, F_{ijk} are components of the strength tensors and FI is the failure index. Failure is predicted when $FI \geq 1$. For practical applications, the terms in equation (8) higher than quadratic are usually set to zero due to the diminishing returns of including higher-order polynomial terms in predicting failure together with the increased cost of experimentally determining these higher–order strength components. In 2–D problems, a problem in tensor polynomial criteria is the 'interaction term', F_{12}, which is constrained by the following 'stability criterion' given in [62] as

$$F_{11}F_{22} - F_{12}^2 > 0 \tag{9}$$

It is argued in [62] that the difficulty in experimentally determining the interaction term, F_{12}, is highly sensitive to experimental measurement in regards to satisfying the above stability criterion. It is demonstrated that the term may be dropped without adversely effecting failure prediction. For the 2–D case, an approach for approximating the interaction term as a function of normal strength measures is presented in [63] which yields

$$F_{12} = -\frac{1}{X_tY_t + X_cY_c} \tag{10}$$

A similar approach is adopted to determine the interaction terms arising in 3–D problems.

Of the various anisotropic failure criteria, the maximum stress criterion is independent of the particular failure mode and ultimate ply failure is predicted when any one of the following conditions are satisfied

$$\begin{array}{lllllll} \sigma_1 & > & X_t; & \sigma_1 & < & X_c; & \sigma_4 > R \\ \sigma_2 & > & Y_t; & \sigma_2 & < & Y_c; & \sigma_5 > S \\ \sigma_3 & > & Z_t; & \sigma_3 & < & Z_c; & \sigma_6 > T \end{array} \tag{11}$$

where σ_1, σ_2 and σ_3 are the normal stress components and σ_4, σ_5 and σ_6 are the shear stress components. The strength measures are given by X_t, X_c, Y_t, Y_c, Z_t and Z_c which are the normal tensile and compressive strengths in the x, y and z directions, respectively, and R, S and T are the shear strengths in the yz, xz and xy planes, respectively. The maximum strain criterion is of identical form as the above with stresses replaced by corresponding strains and strength measures replaced by associated maximum strain measures.

The general Hoffman criterion is given by

$$\begin{aligned} FI &= F_1\sigma_1 + F_2\sigma_2 + F_3\sigma_3 + F_{11}\sigma_1^2 + F_{12}\sigma_1\sigma_2 + F_{13}\sigma_1\sigma_3 + F_{22}\sigma_2^2 + \\ &\quad F_{23}\sigma_2\sigma_3 + F_{33}\sigma_3^2 + F_{44}\sigma_4^2 + F_{55}\sigma_5^2 + F_{66}\sigma_6^2 \end{aligned} \tag{12}$$

where

$$\begin{aligned} F_1 &= \frac{1}{X_t} - \frac{1}{X_c}; \quad F_2 = \frac{1}{Y_t} - \frac{1}{Y_c}; \quad F_3 = \frac{1}{Z_t} - \frac{1}{Z_c} \\ F_{11} &= \frac{1}{X_tX_c}; \qquad F_{22} = \frac{1}{Y_tY_c}; \qquad F_{33} = \frac{1}{Z_tZ_c} \\ F_{44} &= \frac{1}{R^2}; \qquad F_{55} = \frac{1}{S^2}; \qquad F_{66} = \frac{1}{T^2} \\ F_{12} &= -\frac{1}{2}\left(\frac{1}{X_tX_c} + \frac{1}{Y_tY_c} - \frac{1}{Z_tZ_c}\right) \\ F_{13} &= -\frac{1}{2}\left(\frac{1}{X_tX_c} + \frac{1}{Z_tZ_c} - \frac{1}{Y_tY_c}\right) \\ F_{23} &= -\frac{1}{2}\left(\frac{1}{Z_tZ_c} + \frac{1}{Y_tY_c} - \frac{1}{X_tX_c}\right) \end{aligned} \tag{13}$$

For 2–D plane problems the Hoffman criterion is obtained by dropping appropriate terms to yield

$$FI = \left(\frac{1}{X_t} - \frac{1}{X_c}\right)\sigma_1 + \left(\frac{1}{Y_t} - \frac{1}{Y_c}\right)\sigma_2 + \frac{\sigma_1^2}{X_tX_c} + \frac{\sigma_2^2}{Y_tY_c} + \frac{\sigma_{12}^2}{S} - \frac{\sigma_1\sigma_2}{X_tX_c} \tag{14}$$

The general Hill criterion is based on exclusively quadratic terms given by

$$FI = F_{11}\sigma_1^2 + F_{12}\sigma_1\sigma_2 + F_{13}\sigma_1\sigma_3 + F_{22}\sigma_2^2 + F_{23}\sigma_2\sigma_3 + F_{33}\sigma_3^2 + F_{44}\sigma_4^2 + F_{55}\sigma_5^2 + F_6\sigma_6^2 \tag{15}$$

where

$$\begin{aligned} F_{11} &= \frac{1}{X^2}; \qquad F_{22} = \frac{1}{Y^2}; \qquad F_{33} = \frac{1}{Z^2} \\ F_{44} &= \frac{1}{R^2}; \qquad F_{55} = \frac{1}{S^2}; \qquad F_{66} = \frac{1}{T^2} \\ F_{12} &= -\frac{1}{2}\left(\frac{1}{X^2} + \frac{1}{Y^2} - \frac{1}{Z^2}\right) \\ F_{13} &= -\frac{1}{2}\left(\frac{1}{X^2} + \frac{1}{Z^2} - \frac{1}{Y^2}\right) \\ F_{23} &= -\frac{1}{2}\left(\frac{1}{Z^2} + \frac{1}{Y^2} - \frac{1}{X^2}\right) \end{aligned} \tag{16}$$

in which the value for the normal tensile strengths, X, Y and Z, are taken as compressive or tensile

depending on the sign of the corresponding normal stresses.

The general Tsai-Wu criterion is given by

$$\begin{aligned} FI &= F_1\sigma_1 + F_2\sigma_2 + F_3\sigma_3 + F_{11}\sigma_1^2 + F_{12}\sigma_1\sigma_2 + F_{13}\sigma_1\sigma_3 + F_{22}\sigma_2^2 + \\ &\quad F_{23}\sigma_2\sigma_3 + F_{33}\sigma_3^2 + F_{44}\sigma_4^2 + F_{55}\sigma_5^2 + F_{66}\sigma_6^2 \end{aligned} \tag{17}$$

where

$$\begin{aligned} F_1 &= \frac{1}{X_t} - \frac{1}{X_c}; \quad F_2 = \frac{1}{Y_t} - \frac{1}{Y_c}; \quad F_3 = \frac{1}{Z_t} - \frac{1}{Z_c} \\ F_{11} &= \frac{1}{X_t X_c}; \qquad F_{22} = \frac{1}{Y_t Y_c}; \qquad F_{33} = \frac{1}{Z_t Z_c} \\ F_{44} &= \frac{1}{R^2}; \qquad F_{55} = \frac{1}{S^2}; \qquad F_{66} = \frac{1}{T^2} \\ F_{12} &= -\frac{1}{2}(\sqrt{X_t X_c Y_t Y_c}) \\ F_{13} &= -\frac{1}{2}(\sqrt{X_t X_c Z_t Z_c}) \\ F_{23} &= -\frac{1}{2}(\sqrt{Y_t Y_c Z_t Z_c}) \end{aligned} \tag{18}$$

For 2–D plane problems the Tsia–Wu criterion is presented in Reference [64] as

$$FI = F_1\sigma_1 + F_2\sigma_2 + F_{11}\sigma_1^2 + 2F_{12}\sigma_1\sigma_2 + F_{22}\sigma_2^2 + F_{66}\sigma_{12}^2 \tag{19}$$

where

$$\begin{aligned} F_1 &= \frac{1}{X_t} - \frac{1}{X_c} \\ F_2 &= \frac{1}{Y_t} - \frac{1}{Y_c} \\ F_{11} &= -\frac{1}{X_t X_c} \\ F_{22} &= -\frac{1}{Y_t Y_c} \\ F_{12} &= -\frac{1}{X_t Y_t + X_c Y_c} \\ F_{66} &= \frac{1}{S^2} \end{aligned} \tag{20}$$

The above criteria have been successfuly used to predict failure in generally anisotropic materials. One drawback, however, is that without modification these criteria do not predict the underlying failure mode which is important for design purposes. In Reference [53] the basic form of anisotropic failure theories are used to develop criteria to account for specific failure modes of the basic ply constituents such as fiber rupture in tension or buckling in compression and general matrix failure. Recently, ply failure criteria have been proposed accounting for ply nonlinearities and incorporated

into successful analyses of composite failure such as those presented in References [65, 66]. A tensile matrix failure criterion is stated therein as

$$(\frac{\sigma_y}{Y_t})^2 + \frac{\sigma_{xy}^2 + \frac{3}{2}G_{xy}\alpha\sigma_{xy}^4}{S_c^2 + \frac{3}{2}G_{xy}\alpha S_c^4} = e_{mt}^2 \tag{21}$$

where σ_y and σ_{xy} are the layer transverse tensile stress and shear stress, respectively, and Y_t and S_c are the transverse tensile strength and the modified *in situ* shear strength, respectively. Compressive matrix failure may be predicted using the Hashin Failure Criterion [53] which is stated as

$$(\frac{\sigma_y}{2Y_c})^2 + [(\frac{Y_c}{2S_c})^2 - 1]\frac{\sigma_y}{Y_c} + \frac{\sigma_{xy}^2 + \frac{3}{2}G_{xy}\alpha\sigma_{xy}^4}{S_c^2 + \frac{3}{2}G_{xy}\alpha S_c^4} = e_{mc}^2 \tag{22}$$

A modification of the Yamada-Sun failure criteria presented in [65, 66] may be used to predict both fiber-matrix shearing and fiber breakage as given by

$$(\frac{\sigma_x}{X_t})^2 + \frac{\sigma_{xy}^2 + \frac{3}{2}G_{xy}\alpha\sigma_{xy}^4}{S_c^2 + \frac{1}{2}G_{xy}\alpha S_c^4} = e_f^2 \tag{23}$$

where σ_x and X_t are the longitudinal tensile stress and strength in each ply, respectively. In using the above criteria, matrix or fiber failure is predicted when e_{mt}, e_{mc} or $e_f \geq 1$.

Additional failure modes have been identified and examined in the literature. One such mode is a microbuckling phenomenon giving rise to propagating kink bands in ply fiber arrays eventually leading to fiber fracture. As discussed in References [67, 68], such kink bands are precipitated under compressive loading in primary load-carrying plies usually at the free edges which then tend to propagate through the width. The change in strain energy, ΔU, of a unit width kink band is given by

$$\Delta U = (2A_f g_f + \frac{1}{4}d_f\sigma_{ym}l_k^2\theta_k)[\frac{t_k c_f}{A_f}] \tag{24}$$

in which A_f, d_f are the fiber cross-sectional area and diameter, g_f is the critical fiber energy release rate corresponding to the flexural toughness of the fiber, σ_{ym} is the yield stress of the matrix material, l_k and θ_k are the kink zone length and angle of rotation with respect to the fiber axis, t_k is the thickness of the kinked ply layer and c_f is the fiber volume fraction of the kinked ply. Future work is suggested to develop a ply or laminate failure criterion together with a damage law accounting for kink zone development and propogation. This type of damage is dependent on the laminate geometric configuration, loading and support conditions.

The selection of appropriate ply failure criteria is thus an important aspect of the mathematical modeling of residual strength. Any lamina–level criterion which is based on the assumption of a homogeneous ply continuum inevitably introduces an approximation and source of predictive error in the failure analysis of composite laminates.

Ply Strength Measures

The prediction of ply failure in a composite laminate requires an accurate calculation of stress distribution through the laminate thickness together with experimentally determined ply strength measures used in various failure criteria. For isotropic materials, a single strength parameter may

be obtained from a tensile, compressive or shear stress test. Such materials may be referred to as one–dimensional or one–constant material systems. In contrast, composite laminae represented as anisotropic homogeneous materials require several parameters to characterize the failure surface when plotted in stress or strain space. These include compressive and tensile strength along the longitudinal and transverse directions relative to ply fibers, and shear strengths in all principle ply directions. A typical 2-D failure envelope for a composite ply is depicted in Figure 10.

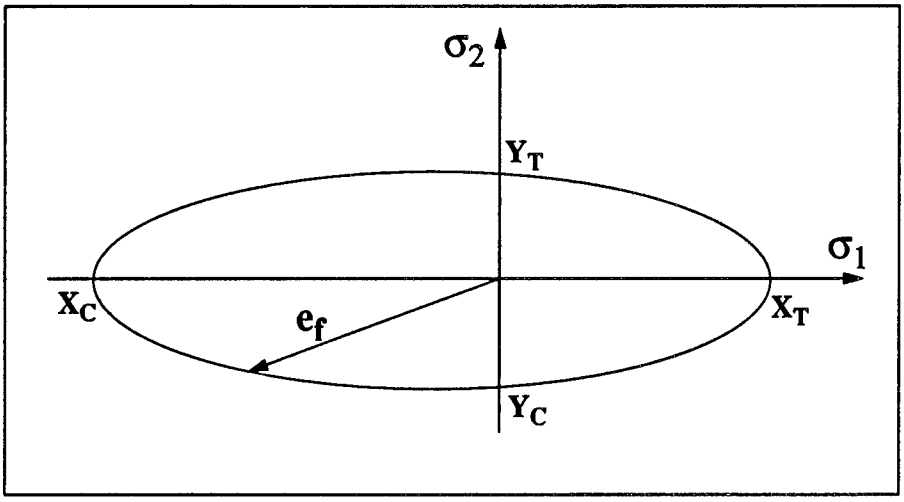

Figure 10. Typical 2-D failure envelope for a composite ply.

Ply strengths are dependent on the basic fiber and matrix properties, fiber distribution and orientation, and on the integrity of the interfacial bonding between the fibers and the matrix [47]. Under a general state of local stress, a number of different, potential weakest–links exist to dictate ply strength. Lamina strengths are most commonly obtained experimentally yet analytical models may be developed to predict strength based on assumptions regarding the applied loading and micromechanical characteristics of the ply constituents. Reference [69] discusses in detail the importance of fiber–matrix bonding characteristics and examines the influence of bond strength at the fiber–matrix interface on ultimate tensile strength by analytically computing strength measures based on progressive fracturing of fibers. A micromechanical equilibrium element model is developed in which an initially assumed cylindrical core of damaged composite is surrounded by a concentric array of undamaged fibers. The result of the analysis yields a relationship for strength of the following form

$$Q_{i+1} = Q_i n_i \left\{ 1 - exp\left[-\lambda_i \left(\frac{\sigma}{\sigma_o} \right)^m \right] \right\} \tag{25}$$

$$\lambda_i = 2 \int_0^{\delta_i} \left[\frac{du_1}{d\xi}(\xi) \right]^m d\xi \tag{26}$$

The derivation of equations (25,26) are fully detailed and all variables defined in Reference [69]; the equations are presented to show the functional form and iterative nature of an analytical determination of ply strengths based on micromechanical elasticity models. In the above, n_i is the

number of nearest-neighbor fibers with i denoting the number of broken fibers. Q_i is the number of broken fiber clusters and λ_i is related to the stress concentration in neighboring fibers. To determine the ply strength, the applied load σ_i is incremented until

$$\sigma_i > \sigma_{i+1} \tag{27}$$

which indicates that the ply tensile strength is given by σ_i since additional applied loading causes an unstable and catastrophic sequence of fiber fracture to occur. Other idealized micromechanical models may be developed to analytically estimate other ply strength measures.

In the experimental determination of ply strengths, various tests are performed using unidirectional laminates in which it is conventionally assumed that the computed strengths are fundamental constants of a particular composite material system. Linear criteria such as maximum stress or maximum strain failure theories assume an independence of longitudinal, transverse and shear strengths thereby simplifying the experimental tests required to determine the composite failure strengths. Quadratic or general tensor polynomial failure criteria incorporate interaction terms which require difficult experimental tests with biaxially loaded test specimens to determine their values. In many cases, however, it has been noted that these interaction terms may be neglected without adversely effecting failure prediction [62].

An important observation noted in Reference [70] states that the past assumption of treating ply strengths as material constants is incorrect but is instead dependent on laminate thickness and ply orientation. A disparity as great as 50% has been observed in calculated ply strengths between experimental results for unidirectional and multi-directional laminates. Other experimental investigations have corroborated laminate dependence on measured strength values. In Reference [71] fiberglass composites demonstrated shear strength values strongly dependent on laminate thickness. In Reference [72] the shear strength of T300/1034-C Graphite/Epoxy prepregs were found to be a function of the volume fraction of 0 degree fibers. Further studies on the difference of *in situ* strength of individual plies which differ from strength determinations made from experimental testing of unidirectional laminates may be found in [65, 73, 74, 53, 75]. This strength variation is attributable to ply orientation, laminate thickness and residual thermal stresses of which a precise functional relationship is currently unavailable. Empirical relationships are presented in [65, 66] which gives expressions for ply transverse tensile and shear strength as

$$Y_t = Y_t^o(1 + \alpha_1 \frac{sin(\Delta\theta)}{N^{\beta_1}}) \tag{28}$$

$$S_t = S_t^o(1 + \alpha_2 \frac{sin(\Delta\theta)}{N^{\beta_2}}) \tag{29}$$

where Y_t and S_t are the *in situ* transverse tensile and shear strengths. Y_t^o and S_t^o are the respective ply strengths obtained from the testing of unidirectional laminates, $\Delta\theta$ is the angular difference between adjacent ply orientations, N is the number of plies in the laminate or sublaminate being considered and α_1, α_2, β_1 and β_2 are experimentally determined constants. Ply compressive strengths are assumed to be of similar form.

The accurate determination of ply strengths is of primary importance in predicting residual strength and further improvements in testing methods and analytical models are needed to better predict *in situ* ply strength values.

Ply Damage Models

Once ply failure is predicted, various damage laws have been developed to account for degradation in the local 3-D material properties. The simplest damage law applied to composite laminae reduces all ply properties to zero if ply failure has been predicted, regardless of predicted damage mode. This assumption is regarded as extreme and more specialized property reductions models have been advanced for the representation of ply damage.

For compressive or tensile matrix failure, References [15, 65] have developed a model in which the in-plane transverse modulus, E_2 and Poisson's ratios μ_{ij} in the damaged ply is set to zero while all other elastic constants are unchanged. This results in the ply stiffness matrix given by:

$$[C] = \begin{bmatrix} E_1 & 0.0 & 0.0 & 0.0 & 0.0 & 0.0 \\ 0.0 & 0.0 & 0.0 & 0.0 & 0.0 & 0.0 \\ 0.0 & 0.0 & E_3 & 0.0 & 0.0 & 0.0 \\ 0.0 & 0.0 & 0.0 & 0.0 & 0.0 & 0.0 \\ 0.0 & 0.0 & 0.0 & 0.0 & G_{13} & 0.0 \\ 0.0 & 0.0 & 0.0 & 0.0 & 0.0 & G_{12} \end{bmatrix} \tag{30}$$

Reference [76] discusses a refinement to the above model which may be regarded as a limiting case for tensile crack density saturation. A continuum mechanics approach is utilized to define material stiffness reductions based on accumulated transverse crack density. Good correlation with experimental data is obtained although some minor alterations are required to maintain symmetry in the stiffness matrix [77, 78].

For fiber failure, Reference [79] presents a model in which it is assumed that in the damaged ply the in-plane transverse modulus, E_2 and Poisson's ratios μ_{ij} are zero while the longitudinal modulus, E_1, and the shear modulus, G_{12}, are reduced according to a micromechanical fiber bundle failure model [17, 80, 81] yielding a Weibull distribution of these properties given by

$$\frac{E_l^r}{E_l} = Exp[-(\frac{A}{A_o})^\beta] \tag{31}$$

$$\frac{G_{lt}^r}{G_{lt}} = Exp[-(\frac{A}{A_o})^\beta] \tag{32}$$

where E_l^r and G_{lt}^r are the reduced values for the tensile and shear modulii, respectively, A is the area of fiber failure predicted by appropriate fiber failure criteria and the reference area, A_o, is the failure interaction zone based on the measured ply tensile strength X_t [17, 80, 81, 82]. β is the Weibull distribution shape parameter dependent on the extent of observed fiber damage. In the determination of the shape parameter, it has been noted that the prediction of ultimate strength is somewhat insensitive to the value of β as a variation of more than 30% had a negligible effect. An alternative approach which avoids the statistical measurement of the fiber strength is presented in

Reference [19]. In this approach a stiffness reduction coefficient, α, is utilized to degrade material properties. This coefficient is experimentally determined and is assumed as a material property constant for the composite material system being used. An 'interactive' degradation model is presented based on a particular use of the Tsai-Wu failure criterion which is expressed as

$$F_i\sigma_i + F_{ij}\sigma_i\sigma_j = FI \tag{33}$$

where FI is the failure index. The stiffness reduction due to damage is based on computing the failure index for each component of stress in turn to determine the mode of damage. Fiber breakage is assumed if $max\{FI(\sigma_i)\}$ is due to σ_1. The damage law for this mode is given by

$$\begin{aligned} \bar{E}_1 &= \alpha E_1 \\ \bar{G}_{13} &= \alpha G_{13} \\ \bar{G}_{12} &= \alpha G_{12} \\ \bar{\nu}_{13} &= \alpha \nu_{13} \\ \bar{\nu}_{12} &= \alpha \nu_{12} \end{aligned} \tag{34}$$

Matrix cracking is assumed if $max\{FI(\sigma_i)\}$ is due to σ_2 or σ_6 and the corresponding damage law for this mode is given by

$$\begin{aligned} \bar{E}_2 &= \alpha E_2 \\ \bar{G}_{23} &= \alpha G_{23} \\ \bar{G}_{12} &= \alpha G_{12} \\ \bar{\nu}_{21} &= \alpha \nu_{21} \\ \bar{\nu}_{23} &= \alpha \nu_{23} \end{aligned} \tag{35}$$

Delamination is assumed if $max\{FI(\sigma_i)\}$ is due to σ_3, σ_4 or σ_5. The damage law for this mode is given by

$$\begin{aligned} \bar{E}_3 &= \alpha E_3 \\ \bar{G}_{23} &= \alpha G_{23} \\ \bar{G}_{13} &= \alpha G_{13} \\ \bar{\nu}_{31} &= \alpha \nu_{31} \\ \bar{\nu}_{32} &= \alpha \nu_{32} \end{aligned} \tag{36}$$

Appropriate thermodynamic constraints are applied to maintain a positive definite material stiffness matrix relating stresses and strains.

Much research has been devoted to the incorporation of microcracking in analyses to determine constitutive relations. An approximate elasticity approach is presented in Reference [83] for developing reduced constitutive relationships due to distributions of cracks. An idealization of a composite laminate is made using the unit cell depicted in Figure 11. The unit cell is composed of two laminae, lamina 1 is assumed to contain a distribution of transverse cracks while lamina 2 is undamaged.

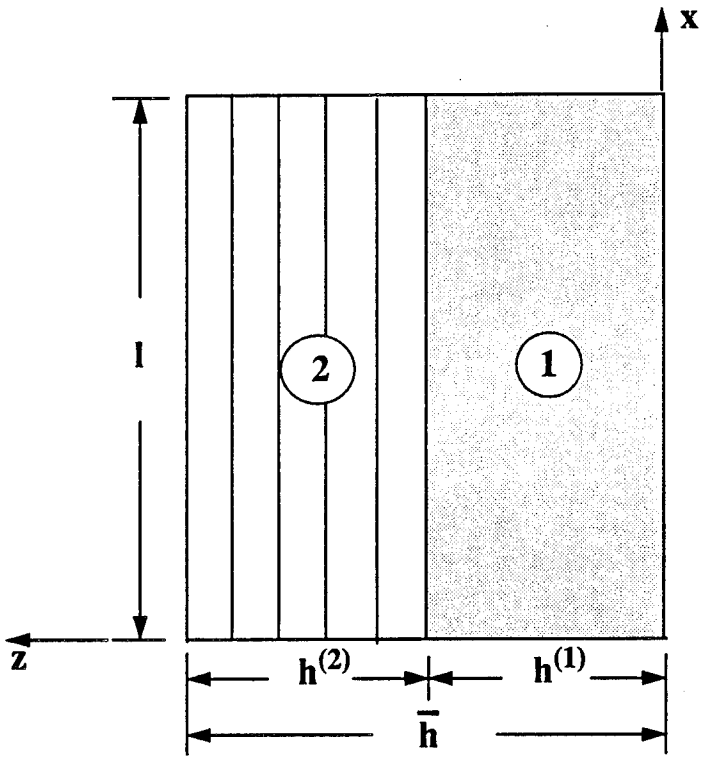

Figure 11. One-quarter unit cell of a composite laminate.

The result of the analysis yields reduced compliance terms for lamina 1 in laminate coordinates given by

$$\begin{Bmatrix} \bar{\epsilon}_x^{(1)} \\ \bar{\epsilon}_y^{(1)} \\ \bar{\gamma}_{xy}^{(1)} \end{Bmatrix} = \begin{bmatrix} \bar{S}_{11}^{(1)} & \bar{S}_{12}^{(1)} & 0 \\ \bar{S}_{12}^{(1)} & \bar{S}_{22}^{(1)} & 0 \\ 0 & 0 & \bar{S}_{66}^{(1)} \end{bmatrix} \begin{Bmatrix} \bar{\sigma}_x^{(1)} \\ \bar{\sigma}_y^{(1)} \\ \bar{\tau}_{xy}^{(1)} \end{Bmatrix} \tag{37}$$

where

$$\begin{aligned} \bar{S}_{11}^{(1)} &= [1 + (\frac{\beta_2 - \beta_1}{\beta_1})(\frac{S_{11}^{(1)} S_{22}^{(1)} - S_{12}^{(1)} S_{12}^{(1)}}{S_{11}^{(1)} S_{22}^{(1)}})] S_{11}^{(1)} \\ \bar{S}_{12}^{(1)} &= S_{12}^{(1)} \\ \bar{S}_{22}^{(1)} &= S_{22}^{(1)} \\ \bar{S}_{66}^{(1)} &= [\frac{\beta_4}{\beta_3}] S_{66}^{(1)} \end{aligned} \tag{38}$$

in which $S_{ij}^{(1)}$ are the undamaged ply compliances in laminate coordinates. The β_i coefficients and reduced stiffness terms, $Q_{ij}^{(1)}$, are given by

$$
\begin{aligned}
\beta_1 &= 1 - \frac{tanh(\alpha_1 l)}{\alpha_1 l} & Q_{11}^{(i)} &= C_{11}^{(i)} - \frac{C_{13}^{(i)} C_{13}^{(i)}}{C_{33}^{(i)}} \\
\beta_2 &= 1 + \frac{h^{(1)} Q_{11}^{(1)}}{h^{(2)} Q_{11}^{(2)}} \frac{tanh(\alpha_1 l)}{\alpha_1 l} & Q_{66}^{(i)} &= C_{66}^{(i)} \\
\beta_3 &= 1 - \frac{tanh(\alpha_2 l)}{\alpha_2 l} & & \\
\beta_4 &= 1 + \frac{h^{(1)} Q_{66}^{(1)}}{h^{(2)} Q_{66}^{(2)}} \frac{tanh(\alpha_2 l)}{\alpha_2 l} & &
\end{aligned}
\tag{39}
$$

where

$$
\alpha_1^2 = \frac{3 C_{55}^{(1)} C_{55}^{(2)}}{h^{(1)} C_{55}^{(2)} + h^{(2)} C_{55}^{(1)}} \frac{h^{(1)} Q_{11}^{(1)} + h^{(2)} Q_{11}^{(2)}}{h^{(1)} h^{(2)} Q_{11}^{(1)} Q_{11}^{(2)}} \tag{40}
$$

$$
\alpha_2^2 = \frac{3 C_{44}^{(1)} C_{44}^{(2)}}{h^{(1)} C_{44}^{(2)} + h^{(2)} C_{44}^{(1)}} \frac{h^{(1)} Q_{66}^{(1)} + h^{(2)} Q_{66}^{(2)}}{h^{(1)} h^{(2)} Q_{66}^{(1)} Q_{66}^{(2)}} \tag{41}
$$

and where l is the crack spacing and $C_{ij}^{(i)}$ are the usual ply stiffness coefficients. An interesting aspect to the developed expressions for reduced lamina compliances is that the compliance terms are not only a function of the elastic constants of the cracked ply but are dependent on the entire laminate construction. Reference [84] presents a micromechanically-based approach for determining reduced compliance terms due to distributed densities of microcracks. Based on the slip theory of plasticity, a superimposition of local constituent properties on planes defined by individual crack orientations is performed to determine macroscopic properties. The resulting constitutive model is given as

$$
\sigma = \mathbf{Q}(\varphi)\epsilon \tag{42}
$$

in which φ is an orientation density function of the cracking planes. The analysis is restricted to 2-D plane assumptions of elasticity and to monotonically increasing tensile loads.

Laminate Analysis

With the aim of developing a numerical procedure to model general 3-D composite laminates, the exact representation of individual plies is considered impractical. 'Exact' solutions to specific laminate problems are obtained through formal application of the mathematical theory of elasticity in which powerful techniques may be applied to obtain solutions for a stratified or discontinuous elastic continuum. These problems are limited to highly idealized geometries which drastically limit their applicability. Instead, the mechanical properties of an assembled laminate may be obtained using a structural engineering approach known as the Classical Laminate Theory (CLT) in which an averaging of ply properties is performed to obtain gross laminate behavior [85, 81]. This approximation permits the modeling of a larger class of laminate problems.

For a 3-D laminate, lamination theory yields the material stiffnesses coefficients, $\mathbf{C}_{ij}$, given by

$$\mathbf{C}_{ij} = \frac{1}{H}\sum_{k=1}^{N} h_k \bar{\mathbf{Q}}_{ij}^k \tag{43}$$

where H is the total laminate thickness, h_k are the individual ply thicknesses and N is the total number of plies. The transformed ply stiffnesses are given by

$$\begin{aligned}
\bar{Q}_{11}^k &= Q_{11}^k cos^4\theta^k + Q_{22}^k sin^4\theta^k + 2Q_{12}^k sin^2\theta^k cos^2\theta^k + 4Q_{66}^k cos^2\theta^k sin^2\theta^k \\
\bar{Q}_{22}^k &= Q_{11}^k sin^4\theta^k + Q_{22}^k cos^4\theta^k + 2(Q_{12}^k + 2Q_{66}^k) sin^2\theta^k cos^2\theta^k \\
\bar{Q}_{33}^k &= Q_{33}^k \\
\bar{Q}_{44}^k &= Q_{44}^k cos^2\theta^k + Q_{55}^k sin^2\theta^k \\
\bar{Q}_{55}^k &= Q_{55}^k cos^2\theta^k + Q_{44}^k sin^2\theta^k \\
\bar{Q}_{66}^k &= Q_{66}^k + (Q_{11}^k + Q_{22}^k - 2Q_{12}^k - 4Q_{66}^k) sin^2\theta^k cos^2\theta^k \\
\bar{Q}_{12}^k &= Q_{12}^k + (Q_{11}^k + Q_{22}^k - 2Q_{12}^k - 4Q_{66}^k) sin^2\theta^k cos^2\theta^k \\
\bar{Q}_{13}^k &= Q_{13}^k cos^2\theta^k + Q_{23}^k sin^2\theta^k \\
\bar{Q}_{23}^k &= Q_{13}^k sin^2\theta^k + Q_{23}^k cos^2\theta^k \\
\bar{Q}_{16}^k &= (Q_{11}^k cos^2\theta^k - Q_{22}^k sin^2\theta^k - cos2\theta^k (Q_{12}^k + 2Q_{66}^k)) cos\theta^k sin\theta^k \\
\bar{Q}_{26}^k &= (Q_{11}^k sin^2\theta^k - Q_{22}^k cos^2\theta^k + cos2\theta^k (Q_{12}^k + 2Q_{66}^k)) sin\theta^k cos\theta^k \\
\bar{Q}_{36}^k &= (Q_{13}^k - Q_{23}^k) sin\theta^k cos\theta^k \\
\bar{Q}_{45}^k &= (Q_{55}^k - Q_{44}^k) sin\theta^k cos\theta^k
\end{aligned} \tag{44}$$

in which

$$\begin{aligned}
Q_{11}^k &= E_1^k(1 - \nu_{23}^k\nu_{32}^k)/(E_2^k E_3^k \Omega^k) \\
Q_{12}^k &= E_2^k(\nu_{12}^k + \nu_{32}^k\nu_{13}^k)/(E_1^k E_3^k \Omega^k) \\
Q_{13}^k &= E_3^k(\nu_{13}^k + \nu_{12}^k\nu_{23}^k)/(E_1^k E_2^k \Omega^k) \\
Q_{22}^k &= E_2^k(1 - \nu_{13}^k\nu_{31}^k)/(E_1^k E_3^k \Omega^k) \\
Q_{23}^k &= E_3^k(\nu_{23}^k + \nu_{21}^k\nu_{13}^k)/(E_1^k E_2^k \Omega^k) \\
Q_{33}^k &= E_3^k(1 - \nu_{12}^k\nu_{21}^k)/(E_1^k E_2^k \Omega^k) \\
Q_{44}^k &= G_{23}^k \\
Q_{55}^k &= G_{31}^k \\
Q_{66}^k &= G_{12}^k
\end{aligned} \tag{45}$$

and

$$\begin{aligned}
\nu_{21}^k &= \nu_{12}^k(E_2^k/E_1^k) \\
\nu_{32}^k &= \nu_{23}^k(E_3^k/E_2^k) \\
\nu_{31}^k &= \nu_{13}^k(E_3^k/E_1^k) \\
\Omega^k &= (1 - \nu_{12}^k\nu_{21}^k - \nu_{23}^k\nu_{32}^k - \nu_{13}^k\nu_{31}^k - 2\nu_{21}^k\nu_{32}^k\nu_{13}^k)
\end{aligned} \tag{46}$$

where E_{ij}, G_{ij}, ν_{ij} and θ are the Young's moduli, shear moduli, Poisson ratios and fiber orientation angle, respectively. The local structural stiffness is thus obtained using the above averaging of individual ply properties. Specific problems may offer a simplification to the above by adopting

plane–stress or plane–strain as mptions in the basic constitutive relations.

An additional assumption im cit to CLT is that of uniform ply thickness. In real laminates, however, plies tend to exhibit 'wavy' distribution of thickness due to nonuniform resin flow during curing which affects the lc al stress distribution. This local perturbation from uniformity is, however, within the order of a proximation inherent to CLT and may be neglected. For common engineering problems involvin built-up composite structures with arbitrary geometries, complex loading and support conditions an approximate CLT representation is the only tractable approach available for use with numeri l techniques such as finite element analysis. Although classical lamination theory is a practic approach for simulating multi-ply laminates, the nature of this mathematical representation a umes an inherent independence of individual plies which has been widely shown through experin ntal and analytical results to be imprecise. As noted above in the discussion of various lamina p perties, ply strength measures and constitutive laws for damaged plies are all *laminate*-dependen Thus, the complexity of laminate analysis is ever present and corrections need to be introduced t the ply level to improve the accuracy of laminate theory without having to resort to the nearly tractable 3-D elasticity representations of general laminates under complex loading and support nditions.

Modeling failure phenomena the laminate level involves the growth of local regions of fiber breakage and matrix cracking plies which coalesce to form significant 3-D regions of damaged laminate material together wi the extension of interply delaminations all of which contribute to ultimate component failure. C mponent level failures are generally characterized as compressive, tensile or local/global buckling odes. The predominant failure modes are dependent on the applied load conditions; under tensile ading, fiber breakage and delamination growth causing significant strain redistribution are the e ential modes involved in failure while under compressive loading matrix cracking, fiber breakag and local delamination buckling become the predominant failure modes. Simulating the gross b avior of the composite component in regards to load–displacement response and local stress reco ry may additionally involve nonlinear material and geometric response under applied loads an potential delamination growth.

The following subsections disc s laminate–level behavior involving laminate failure modes, nonlinear load–displacement respons and delamination instability or buckling failure. It is these effects involving the gross laminate r ponse to applied loads and accumulated damage which must ultimately be simulated and asses d to predict catastrophic component failure.

Laminate Material Failu

A multitude of failure criteria for isotropic materials have been developed which include single component criteria such as ma imum stress, maximum strain and combined stress measures such as Von Mises and Tresca based n distortional energy measures. None of these theories differentiate between compression and tens n and utilize a single parameter - the yield strength - to predict failure. The anisotropic failur criteria such as the Hoffman, Tsai-Hill and Tsai-Wu as discussed above can be applied in an app oximate sense utilizing transformed and averaged ply strengths together with laminate stresses. onservative approximations of local laminate failure have utilized the first ply failure (FPF) crit ia for predicting local/global laminate failure. These criteria, how-

ever, are applied using the state of stress/strain at a point. For the prediction of complete laminate failure, global criteria are required to assess the integrity of composite components. Local regions of material damage cause a general redirection of load 'flow' around regions of reduced stiffness as depicted in Figure 12.

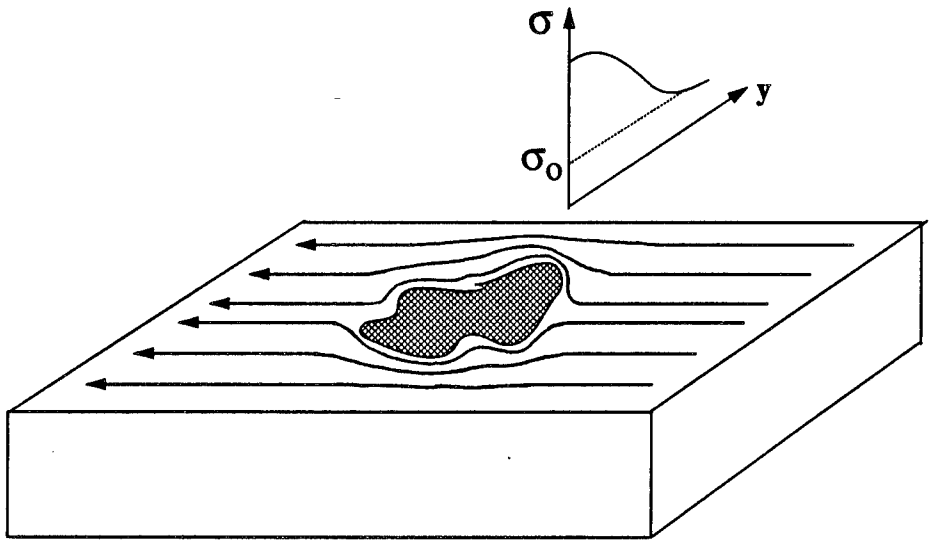

Figure 12. Load redistribution due to local material stiffness loss.

The redistribution of load thereby intesifies the state of stress in adjacent areas and tends to precipitate additional material failure or enhance delamination growth leading to buckling failure.

Laminate level failure criteria may, therefore, be based on gross measures of maximum strains under applied tensile or compressive loading or reduction in flexural stiffness. In an analytical simulation, significant reductions in stiffness along any cross-sectional plane could be used to indicate catastrophic failure. Alternatively, distributed damage resulting in excessive strain or a drop in the integrated resistance to applied loading throughout any cross section may be considered as indicative of ultimate component failure.

Nonlinear Laminate Behavior

Nonlinear laminate behavior may be manifest in geometric nonlinearity involving large displacements and buckling or in material behavior involving nonlinear elastic, viscoelastic and/or plastic response to applied loads. The current study neglects inelastic ply material response and assumes, at most, a nonlinearily elastic behavior to failure. Ply level nonlinear material behavior dictate the global elastic behavior of the composite component. As mentioned in Section 3.2, nonlinearity is primarily observed in the ply shear modulus. In averaging individual ply properties, general

cross-ply laminates such as [±45] layups demonstrate significant nonlinear laminate response while quasi-isotropic layups such as [0/ ± 45/90] behave linearily. Thus, some discretion is available to the analyst in the choice of linear or nonlinear representation of gross laminate behavior based on laminate ply composition. For arbitrary laminates, stress analyses must account for the nonlinear load-displacement behavior of the laminate which requires an iterative solution scheme for all but the simplest geometries. In addition, large displacements constitute a nonlinear geometric response which must be accounted for in analytical simulation by including nonlinear terms in the stress-strain relations. In real materials, both nonlinear material and geometric responses are generally significant in predicting the response to extreme applied loading in order to accurately calculate stresses for residual/failure strength prediction. Analytic or numerical modeling approaches are, therefore, tremendously complicated by these nonlinear effects in obtaining accurate solutions.

Laminate Delamination: Initiation, Buckling and Stability

Under compressive loading, debonding of adjacent plies or delaminations may be considered as the most severe form of laminate damage in contributing to the reduction in residual strength through local buckling failure and flexural stiffness reduction. In addition to the presence of initial delaminations due to manufacturing defects or impact events, laminate stresses can initiate and propagate new delaminations. Numerous criteria have been developed to predict the initiation of delaminations [86, 87, 88]. For example, Reference [89] presents a quadratic delamination criterion of the following form

$$FI = \left(\frac{\bar{\sigma}_{13}{}^2}{Z_{s1}}\right) + \left(\frac{\bar{\sigma}_{23}{}^2}{Z_{s2}}\right) + \left(\frac{\bar{\sigma}^t_{33}{}^2}{Z_t}\right) + \left(\frac{\bar{\sigma}^c_{13}{}^2}{Z_c}\right) \tag{47}$$

where all stresses are average measures computed as

$$\bar{\sigma}_{ij} = \frac{1}{X_{ave}} \int_0^{X_{ave}} \sigma_{ij} dx \tag{48}$$

where X_{ave} is a characteristic length either assumed or determined experimentally. The strength parameters are given as

Z_t = tensile interlaminar normal strength.
Z_c = compressive interlaminar normal strength.
Z_{s1} = interlaminar shear strength for σ_{13} stresses.
Z_{s2} = interlaminar shear strength for σ_{23} stresses.

Local buckling of laminate sublayers, as depicted in Figure 13, can create high interlaminar stresses at the delamination fronts which may cause further extention of the buckled layer. Consequentially, the redistribution of loads may induce additional delaminations and inplane material damage.

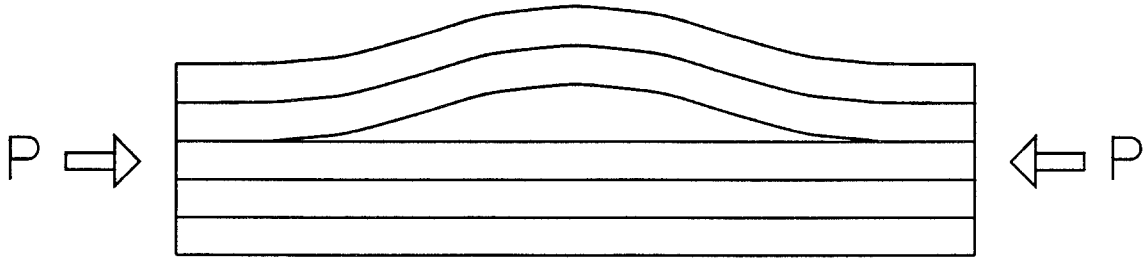

Figure 13. Local buckling of sublaminate due to delamination.

Delaminations may be formed during laminate construction, through microcrack coalescence under service fatigue loading or through impact with foreign objects. In built-up laminates it has been noted that delamination due to impact tends not to occur between plies of like orientation [90, 8]. Various analytical models have been developed using structural engineering approximations such as beams and plates to represent laminate sublayers [6, 10, 7, 11], and approximate elasticity solution approaches have been formulated in [9, 11] using energy methods. Other investigations have utilized specialized finite element analyses which have determined that the stress state around delaminated regions is generally biaxial and that, depending on ply layup and delamination configuration, buckling can initiate under applied tensile loading [6, 11, 12]. Additional effects which have been studied involve bridging between delamination surfaces due to fibers or stitching repair [91].

Buckling or structural instability may be defined as the condition at which the change in the total potential energy associated with an arbitrary displacement, δq, from equilibrium is an extremum or, equivalently, that the total potential satisfies the Trefftz criterion [92] given by

$$\Pi = \mathbf{U} + \mathbf{V} \tag{49}$$

and

$$\frac{\delta^2 \Pi}{\delta \phi^2} = 0 \tag{50}$$

in which U is the total strain energy, V is the potential energy and ϕ is the generalized displacement. Crack stability leading to delamination growth has been most successfuly investigated using a fracture mechanics approach [11, 93, 94]. The basic Griffith energy criteria for crack growth may be stated as

$$\frac{d}{da}(\mathbf{W} - \mathbf{U}) = \mathbf{G}_c \tag{51}$$

where $\mathbf{W}$ is the work performed by external applied loading, $\mathbf{U}$ is the internal elastic strain energy, $\mathbf{G}_c$ is the critical strain energy release rate required to create new fracture surface and a is the initial crack length. A versatile technique for calculating the strain energy release rate with ideal finite element suitability is the crack-closure integral method [95, 96]. The essential idea is that the

energy absorbed in extending a crack by an amount Δa is equal to the work required to close the crack to its original length. The energy statement may be expressed as

$$\mathbf{G} = \mathbf{G}_I + \mathbf{G}_{II} \tag{52}$$

where $\mathbf{G}$ is the total strain energy release rate and $\mathbf{G}_I$ and $\mathbf{G}_{II}$ are the energy release rates associated with Mode I and Mode II deformation components. With the polar coordinate system depicted in Figure 14, the strain energy release rate components may be expressed as

$$\mathbf{G}_I = \lim_{\Delta a \to 0} \frac{1}{2\Delta a} \int_0^{\Delta a} \sigma_y(\Delta a - r, 0)\bar{v}(r, \pi)dr \tag{53}$$

$$\mathbf{G}_{II} = \lim_{\Delta a \to 0} \frac{1}{2\Delta a} \int_0^{\Delta a} \tau_{xy}(\Delta a - r, 0)\bar{u}(r, \pi)dr \tag{54}$$

where σ_y and τ_{xy} are stresses near the crack tip - or delamination front, $\bar{u}$ and $\bar{v}$ are the relative Mode I sliding and Mode II opening displacements between opposing points along the crack length and Δa is the incremental extension in the initial crack length, a.

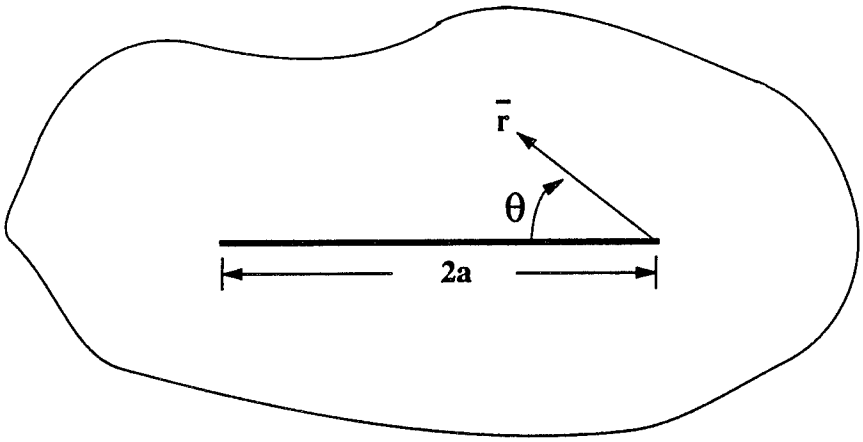

Figure 14. Coordinate system at crack front

The presence of an initial profile of delaminations through the laminate thickness may, thus, exhibit growth during subsequently applied loads due to coupling between buckling and crack instability leading to component failure. In purely structural instability situations in which growth of initial delaminations is not predicted, local buckling may couple with global buckling to cause failure through a 'mixed-mode' instability.

Finite Element Modelling

Numerous specialized analytical approaches to predicting residual strength in composite materials have been made incorporating specific failure modes and highly idealized geometric configurations.

The finite element method provides a completely generic numerical approach to potentially incorporate all salient material behavior and failure modes while allowing arbitrary geometries, applied loads and support conditions to be incorporated in the analysis [97]. The present study is ultimately directed towards simulating impact damage in thick laminated composites which immediately suggest plate–type finite element formulations to represent the elastic continuum. In the domain of single–layer representations simple first–order shear deformable theories such as presented in Reference [98] or higher–order formulations such as those presented in References [100-103] may be considered. However, an important consideration is the representation of three dimensional effects in any plate formulation. Reference [103] presents a viable equivalent single–layer plate theory incorporating three–dimensional behavior while requiring exclusively Poisson-type boundary conditions. Layer-wise theories have been developed such as those of References [104, 105] which attempt to account in greater detail for variations through the laminate thickness. One drawback, however, inherent to all plate formulations is the impossibility of representing delamination growth and local sublaminate buckling which may be a dominant failure mode in certain laminate types and damage distributions. Therefore, for maximum versatility in three dimensional modeling of thick laminates, an 8–node solid brick element is suggested which utilizes the hybrid stress technique to represent elastic stiffness response while purely displacement-based field assumptions are used to develop differential stiffness relations to model geometric nonlinear response. Material degradation due to sequential failures is determined using the above failure criteria together with assumed ply damage laws and is directly incorporated into the element formulation. The basic element formulations together with nonlinear material and geometric solution algorithms are presented in the following subsections.

Elastic Stiffness Formulation

The hybrid stress technique is utilized to form elastic stiffness relationships. Details on the hybrid method may be found in References [108-114]. The structure of element matrices are defined by the energy functional which is selected as the extended Hellinger-Reissner functional and may be stated as

$$\Pi_R = \int_v [(-1/2)\boldsymbol{\sigma}^T \mathbf{S}\boldsymbol{\sigma} + \boldsymbol{\sigma}^T(\mathbf{L}\mathbf{u}_q) - (\mathbf{L}^T\boldsymbol{\sigma})^T\mathbf{u}_\lambda]dv \tag{55}$$

where $\boldsymbol{\sigma}$ is the assumed stress field, $\mathbf{S}$ is the material compliance matrix, $\mathbf{u}_q$ and $\mathbf{u}_\lambda$ are the assumed compatible and incompatible displacement fields, and $\mathbf{L}$ is the differential operator relating strains to displacements.

The assumed stresses may be represented by

$$\boldsymbol{\sigma} = \boldsymbol{P}\boldsymbol{\beta} \tag{56}$$

where $\mathbf{P}$ is a matrix of polynomial terms and $\boldsymbol{\beta}$ is a vector of undetermined expansion coefficients. The displacement field is assumed over the element domain as

$$\mathbf{u} = \mathbf{u}_q + \mathbf{u}_\lambda \tag{57}$$

in which compatible and incompatible displacement components are given by

$$\mathbf{u}_q = \mathbf{N}\mathbf{q} \tag{58}$$

$$\mathbf{u}_\lambda = \mathbf{M}\boldsymbol{\lambda} \tag{59}$$

where $\mathbf{N}$ and $\mathbf{M}$ are compatible and incompatible displacement shape functions, respectively, $\mathbf{q}$ are nodal displacements, and $\boldsymbol{\lambda}$ are Lagrange multipliers which enforce internal constraints. In the form of (55), performing the variation with respect to $\mathbf{u}_\lambda$, the incompatible displacements may be used to variationally enforce *a priori* the field equilibrium conditions through the last term in (55) which requires that

$$\delta \int_v (\mathbf{L}^T \boldsymbol{\sigma})^T \mathbf{u}_\lambda dv = 0 \tag{60}$$

or

$$\mathbf{L}^T \boldsymbol{\sigma} = 0 \tag{61}$$

Applying the constraints to the stress modes results in the reduced functional

$$\Pi_R = \int_v [(-1/2)\boldsymbol{\sigma}^T \mathbf{S} \boldsymbol{\sigma} + \boldsymbol{\sigma}^T (\mathbf{L}\mathbf{u}_q)] dv \tag{62}$$

Substituting (56), (58) and (59) into (55) yields

$$\Pi_R = \int_v [(-1/2)\boldsymbol{\beta}^T \mathbf{P}^T \mathbf{S} \mathbf{P} \boldsymbol{\beta} + \boldsymbol{\beta}^T \mathbf{P}^T (\mathbf{L}\mathbf{N})\mathbf{q}] dv \tag{63}$$

or

$$\Pi_R = (-1/2)\boldsymbol{\beta}^T \mathbf{H} \boldsymbol{\beta} + \boldsymbol{\beta}^T \mathbf{G}\mathbf{q} \tag{64}$$

where

$$\mathbf{H} = \int_v \mathbf{P}^T \mathbf{S} \mathbf{P} dv \tag{65}$$

$$\mathbf{G} = \int_v \mathbf{P}^T (\mathbf{L}\mathbf{N}) dv = \int_v \mathbf{P}^T \mathbf{B} dv \tag{66}$$

Seeking a stationary value of the functional by taking the first variation with respect to $\boldsymbol{\beta}$ yields

$$\boldsymbol{\beta} = \mathbf{H}^{-1} \mathbf{G}\mathbf{q} \tag{67}$$

substituting the resulting expression for $\boldsymbol{\beta}$ into (64), the variation with respect to $\mathbf{q}$ yields the element stiffness matrix as

$$\mathbf{K} = \mathbf{G}^T \mathbf{H}^{-1} \mathbf{G} \tag{68}$$

An 8–node solid element as depicted in Figure 15 is selected to represent the laminate continuum.

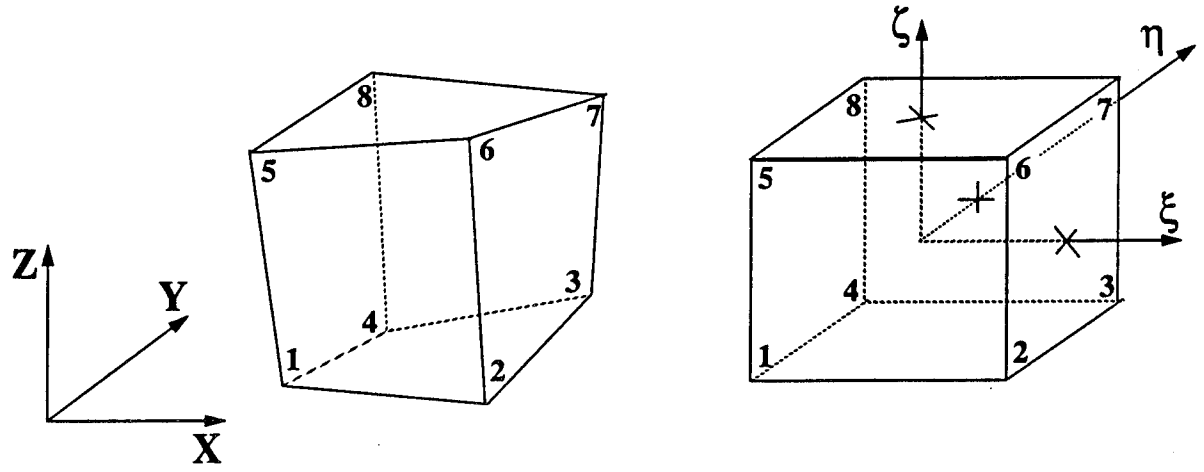

Figure 15. Hexahedral element configuration.

The displacement functions $\mathbf{u}_q$ are given by

$$\mathbf{u}_q = \left\{ \begin{array}{c} u_q \\ v_q \\ w_q \end{array} \right\} = \sum_{i=1}^{8} \frac{1}{8}(1+\xi_i\xi)(1+\eta_i\eta)(1+\zeta_i\zeta) \left\{ \begin{array}{c} u_i \\ v_i \\ w_i \end{array} \right\} \tag{69}$$

The isoparametric mapping between physical and natural coordinates is given by

$$\begin{array}{rcl} x &=& a_0 + a_1\xi + a_2\eta + a_3\zeta + a_4\xi\eta + a_5\xi\zeta + a_6\eta\zeta + a_7\xi\eta\zeta \\ y &=& b_0 + b_1\xi + b_2\eta + b_3\zeta + b_4\xi\eta + b_5\xi\zeta + b_6\eta\zeta + b_7\xi\eta\zeta \\ z &=& c_0 + c_1\xi + c_2\eta + c_3\zeta + c_4\xi\eta + c_5\xi\zeta + c_6\eta\zeta + c_7\xi\eta\zeta \end{array} \tag{70}$$

where

$$\begin{bmatrix} a_0 & b_0 & c_0 \\ a_1 & b_1 & c_1 \\ a_2 & b_2 & c_2 \\ a_3 & b_3 & c_3 \\ a_4 & b_4 & c_4 \\ a_5 & b_5 & c_5 \\ a_6 & b_6 & c_6 \\ a_7 & b_7 & c_7 \end{bmatrix} = \frac{1}{8} \begin{bmatrix} 1 & 1 & 1 & 1 & 1 & 1 & 1 & 1 \\ -1 & 1 & 1 & -1 & -1 & 1 & 1 & -1 \\ -1 & -1 & 1 & 1 & -1 & -1 & 1 & 1 \\ -1 & -1 & -1 & -1 & 1 & 1 & 1 & 1 \\ 1 & -1 & 1 & -1 & 1 & -1 & 1 & -1 \\ 1 & -1 & -1 & 1 & -1 & 1 & 1 & -1 \\ 1 & 1 & -1 & -1 & -1 & -1 & 1 & 1 \\ -1 & 1 & -1 & 1 & 1 & -1 & 1 & -1 \end{bmatrix} \begin{bmatrix} x_1 & y_1 & z_1 \\ x_2 & y_2 & z_2 \\ x_3 & y_3 & z_3 \\ x_4 & y_4 & z_4 \\ x_5 & y_5 & z_5 \\ x_6 & y_6 & z_6 \\ x_7 & y_7 & z_7 \\ x_8 & y_8 & z_8 \end{bmatrix} \tag{71}$$

The stress field is initially assumed as complete quadratic expansions in natural or tensor coordinates given by

$$\boldsymbol{P} = \begin{bmatrix} [\boldsymbol{P}_o] & & & & & \\ & [\boldsymbol{P}_o] & & & & \\ & & [\boldsymbol{P}_o] & & & \\ & & & [\boldsymbol{P}_o] & & \\ & & & & [\boldsymbol{P}_o] & \\ & & & & & [\boldsymbol{P}_o] \end{bmatrix} \tag{72}$$

where

$$[\mathbf{P}_0] = [1, \xi, \eta, \zeta, \xi\eta, \eta\zeta, \zeta\xi, \xi^2, \eta^2, \zeta^2] \tag{73}$$

As detailed in Reference [110], incompatible displacement functions are assumed such that the polynomial order the total displacement field is cubic thereby yielding a resultant quadratic strain field of the same order as the assumed stresses. The assumed stress modes are then subjected to the constraint given by equation (61) yielding an element stress field with 18 independent stress modes given by

$$\begin{array}{rcl} \tau^{11} &=& \beta_1 + \beta_2\eta + \beta_3\zeta + \beta_4\eta\zeta \\ \tau^{22} &=& \beta_5 + \beta_6\xi + \beta_7\zeta + \beta_8\xi\zeta \\ \tau^{33} &=& \beta_9 + \beta_{10}\xi + \beta_{11}\eta + \beta_{12}\xi\eta \\ \tau^{23} &=& \beta_{13} + \beta_{14}\zeta \\ \tau^{31} &=& \beta_{15} + \beta_{16}\xi \\ \tau^{12} &=& \beta_{17} + \beta_{18}\eta \end{array} \tag{74}$$

To preserve the constant stress terms, the natural stresses are mapped to physical space through a contravariant transformation using Jacobians computed at the element centroid

$$\sigma^{kl} = (J_o)^k_i (J_o)^l_j \tau^{ij} \tag{75}$$

The stress field expressed in physical or Cartesian coordinates is given by

$$P = \left[\begin{array}{ccc} [P_1] & [P_2] & [P_3] \end{array} \right] \tag{76}$$

where

$$[P_1] = \begin{bmatrix} 1.0 & 0.0 & 0.0 & 0.0 & 0.0 & 0.0 \\ 0.0 & 1.0 & 0.0 & 0.0 & 0.0 & 0.0 \\ 0.0 & 0.0 & 1.0 & 0.0 & 0.0 & 0.0 \\ 0.0 & 0.0 & 0.0 & 1.0 & 0.0 & 0.0 \\ 0.0 & 0.0 & 0.0 & 0.0 & 1.0 & 0.0 \\ 0.0 & 0.0 & 0.0 & 0.0 & 0.0 & 1.0 \end{bmatrix} \tag{77}$$

$$[P_2] = \begin{bmatrix} a_1^2\eta & a_1^2\zeta & a_2^2\xi & a_2^2\zeta & a_3^2\xi & a_3^2\eta \\ b_1^2\eta & b_1^2\zeta & b_2^2\xi & b_2^2\zeta & b_3^2\xi & b_3^2\eta \\ c_1^2\eta & c_1^2\zeta & c_2^2\xi & c_2^2\zeta & c_3^2\xi & c_3^2\eta \\ b_1c_1\eta & b_1c_1\zeta & b_2c_2\xi & b_2c_2\zeta & b_3c_3\xi & b_3c_3\eta \\ a_1c_1\eta & a_1c_1\zeta & a_2c_2\xi & a_2c_2\zeta & a_3c_3\xi & a_3c_3\eta \\ a_1b_1\eta & a_1b_1\zeta & a_2b_2\xi & a_2b_2\zeta & a_3b_3\xi & a_3b_3\eta \end{bmatrix} \tag{78}$$

$$[P_3] = \begin{bmatrix} 2a_1a_2\zeta & 2a_2a_3\xi & 2a_1a_3\eta & a_1^2\eta\zeta & a_2^2\xi\zeta & a_3^2\xi\eta \\ 2b_1b_2\zeta & 2b_2b_3\xi & 2b_1b_3\eta & b_1^2\eta\zeta & b_2^2\xi\zeta & b_3^2\xi\eta \\ 2c_1c_2\zeta & 2c_2c_3\xi & 2c_1c_3\eta & c_1^2\eta\zeta & c_2^2\xi\zeta & c_3^2\xi\eta \\ (b_2c_1+b_1c_2)\zeta & (b_2c_3+b_3c_2)\xi & (b_1c_3+b_3c_1)\eta & b_1c_1\eta\zeta & b_2c_2\zeta\xi & b_3c_3\xi\eta \\ (a_2c_1+a_1c_2)\zeta & (a_2c_3+a_3c_2)\xi & (a_1c_3+a_3c_1)\eta & a_1c_1\eta\zeta & a_2c_2\zeta\xi & a_3c_3\xi\eta \\ (a_2b_1+a_1b_2)\zeta & (a_2b_3+a_3b_2)\xi & (a_1b_3+a_3b_1)\eta & a_1b_1\eta\zeta & a_2b_2\zeta\xi & a_3b_3\xi\eta \end{bmatrix} \tag{79}$$

The above 8–node solid element formulation based on hybrid element theory is a robust element with excellent behavior in normal and bending deformation modes.

Geometric Stiffness Formulation

With the discretized geometry inherent to the finite element technique, the effects of nonlinear strains may be represented by discrete matrix formulations based on the current stress state. The geometric stiffness matrix is formulated using the assumed displacement fields in (69) and is given by

$$[\mathbf{K}_\sigma] = \int_v [\mathbf{B}_{NL}]^T [\mathbf{\Gamma}] [\mathbf{B}_{NL}] dv \tag{80}$$

where

$$[\mathbf{\Gamma}] = \begin{bmatrix} [\mathbf{S}] & \mathbf{0} & \mathbf{0} \\ \mathbf{0} & [\mathbf{S}] & \mathbf{0} \\ \mathbf{0} & \mathbf{0} & [\mathbf{S}] \end{bmatrix} \tag{81}$$

and

$$[\mathrm{S}] = \begin{bmatrix} \sigma_{xx0} & \tau_{xy0} & \tau_{zx0} \\ \tau_{xy0} & \sigma_{yy0} & \tau_{yz0} \\ \tau_{xz0} & \tau_{yz0} & \sigma_{zz0} \end{bmatrix} \tag{82}$$

The B_{NL} matrix is given by

$$[\mathrm{B}_{NL}] = \begin{bmatrix} [\mathrm{G}] & \mathbf{0} & \mathbf{0} \\ \mathbf{0} & [\mathrm{G}] & \mathbf{0} \\ \mathbf{0} & \mathbf{0} & [\mathrm{G}] \end{bmatrix} \tag{83}$$

where

$$[\mathrm{G}] = \begin{bmatrix} \mathrm{N}_{1,x} & \mathbf{0} & \mathbf{0} & \mathrm{N}_{2,x} & \ldots & \mathrm{N}_{8,x} \\ \mathrm{N}_{1,y} & \mathbf{0} & \mathbf{0} & \mathrm{N}_{2,y} & \ldots & \mathrm{N}_{8,y} \\ \mathrm{N}_{1,z} & \mathbf{0} & \mathbf{0} & \mathrm{N}_{2,z} & \ldots & \mathrm{N}_{8,z} \end{bmatrix} \tag{84}$$

The modeling of nonlinear strain response may be extended to include large strain and displacement behavior through selection of standard algorithmic solution procedures in the finite element method [113, 115]. These methods involve iterative procedures utilizing total or updated Lagrangian representations of the structural model kinematics.

Delamination Propagation

As discussed above in section 4.3, the crack-closure integral method [95, 96] may be used for calculating the strain energy associated with potential delamination propagation. A particularily attractive feature of this technique is the ability to use a coarse mesh without recourse to singularity elements to obtain accurate measures of the strain energy release rate. Within a standard finite element approximation framework, the evaluation of strain energy release rates is based on nodal forces and displacements. The delamination is represented by a surface of coincident nodes which are used to create a plane of discontinuity through the definition of element connectivities. A representative finite element discretization in the region of the crack tip is shown in Fiqure 16. The work required to close the incremental growth in the crack length may be expressed as

$$\mathrm{G}_I = \lim_{\Delta a \to 0} \frac{1}{2\Delta a} \bar{\mathrm{F}}_a (v_c - v_d) \tag{85}$$

and

$$\mathrm{G}_{II} = \lim_{\Delta a \to 0} \frac{1}{2\Delta a} \bar{\mathrm{T}}_a (u_c - u_d) \tag{86}$$

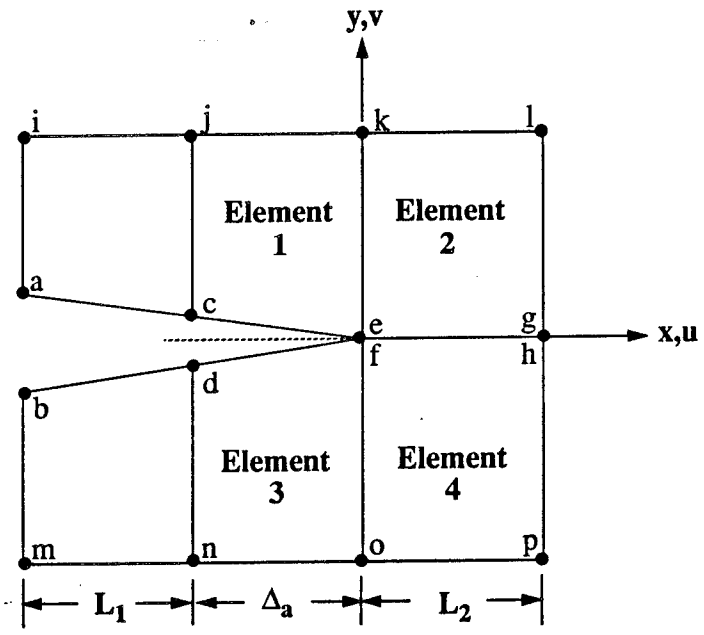

Figure 16. Finite element model of delamination front.

In the computation of the x- and y- nodal forces required to hold the nodes at c and d together, the values for $\mathbf{F}_c$ and $\mathbf{T}_c$ are approximated by the nodal forces at nodes e and f assuming an inverse square root singular behavior near the crack tip as

$$\mathbf{F}_c = (\frac{\Delta a}{l_2})^{1/2}\mathbf{F}_e \tag{87}$$

and

$$\mathbf{T}_c = (\frac{\Delta a}{l_2})^{1/2}\mathbf{T}_e \tag{88}$$

Delamination growth is thus predicted when the release of elastic energy associated with the extension of the delamination exceeds the critical strain energy release rate of the material such that

$$\mathbf{G} = G_I + G_{II} \geq G_C \tag{89}$$

When the above criterion is met, the local delamination front is extended at the evaluation node and incorporated into the model.

The accurate prediction of delamination growth requires a local refinement of the finite element model at the delamination front. Predicting sequential growth at potentially multiple delaminations implies a high degree of mesh refinement and iteration in which the connectivity of the finite element model is updated to account for delamination extension. The crack closure technique does permit a degree of coarseness at the crack tip as demonstrated in Reference [95] in which ratios of incremental crack extension, Δc, to total crack length, c, up to 20% yielded inaccuracies less than 6%. Further study is required to extend the above crack closure methodology to bimaterial interface problems which possess a general λ – order singularity. Additional investigation is warrented

to compare the computational requirements with accuracy in predicting sequential delamination growth in multiply delaminated laminates.

Material Nonlinearity Solution Algorithm

Assuming infinitesimal displacements and small strains, at some applied load level, $\mathbf{P}_a$, the stress/strain relationship may be expressed as

$$\sigma^k = \mathbf{C}^k(\epsilon)\epsilon^k \tag{90}$$

where $C^k(\epsilon)$ is the strain dependent material stiffness matrix, σ^k and ϵ^k are the stress and strain vectors at the k^{th} load level. To solve the nonlinear global nonlinear system of equations, a Newton-Raphson sheme may be employed in which an iterative approach is used to obtain the equilibrium state

$$\mathbf{K}_i\Delta\mathbf{D}_{i+1} = \mathbf{P}_a - \mathbf{R}_i \tag{91}$$

$$\mathbf{D}_{i+1} = \mathbf{D}_i + \Delta\mathbf{D}_{i+1} \tag{92}$$

where $\mathbf{K}_i$ is the elastic stiffness matrix at the i^{th} iteration, $\mathbf{P}_a$ are the applied loads, $\mathbf{R}_i$ are the current internal recovered loads and $\Delta\mathbf{D}_{i+1}$ are the incremental displacements which are summed to give the total displacements for the i^{th} iteration. This scheme is depicted in Figure 17.

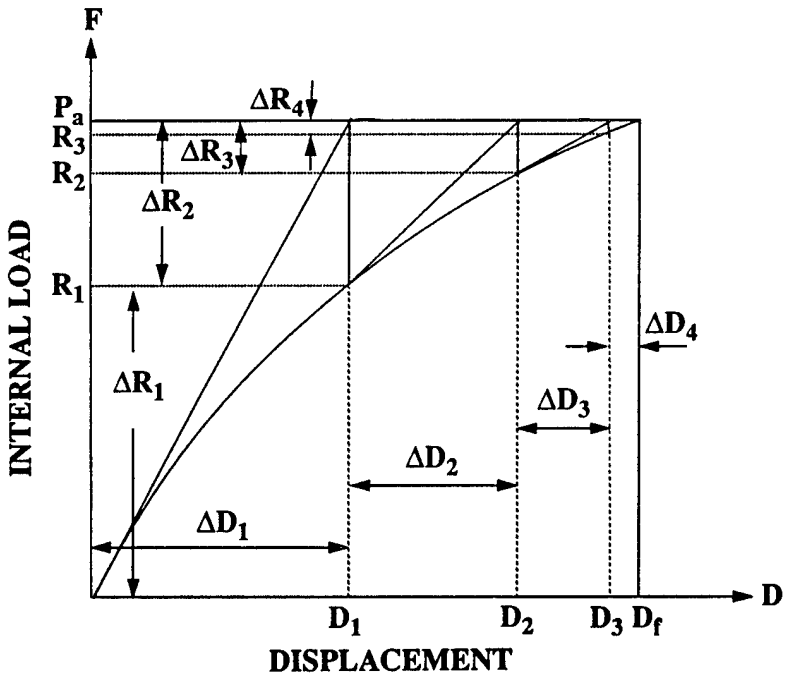

Figure 17. Newton-Raphson iteration scheme.

Iterations are continued until the difference between the vector norms of the externally applied loads and the internal recovered loads are less than a prescribed tolerance

$$|\mathbf{P}_a - \mathbf{R}_i| \leq Tol \tag{93}$$

Convergence rates may be enhanced by performing line searches in the current 'Newton' direction defined by $\Delta\mathbf{D}_{i+1}$ such that

$$\mathbf{D}_{i+1} = \mathbf{D}_i + \beta\Delta\mathbf{D}_{i+1} \tag{94}$$

where β is determined through line search methods such as bisection, secant, Ridder or *Regula Falsi* [113, 115, 116].

Geometric Nonlinear Solution Algorithm

In the linear theory of buckling, a solution is sought at the point where the locus of equilibrium states bifurcate as depicted in Figure 18.

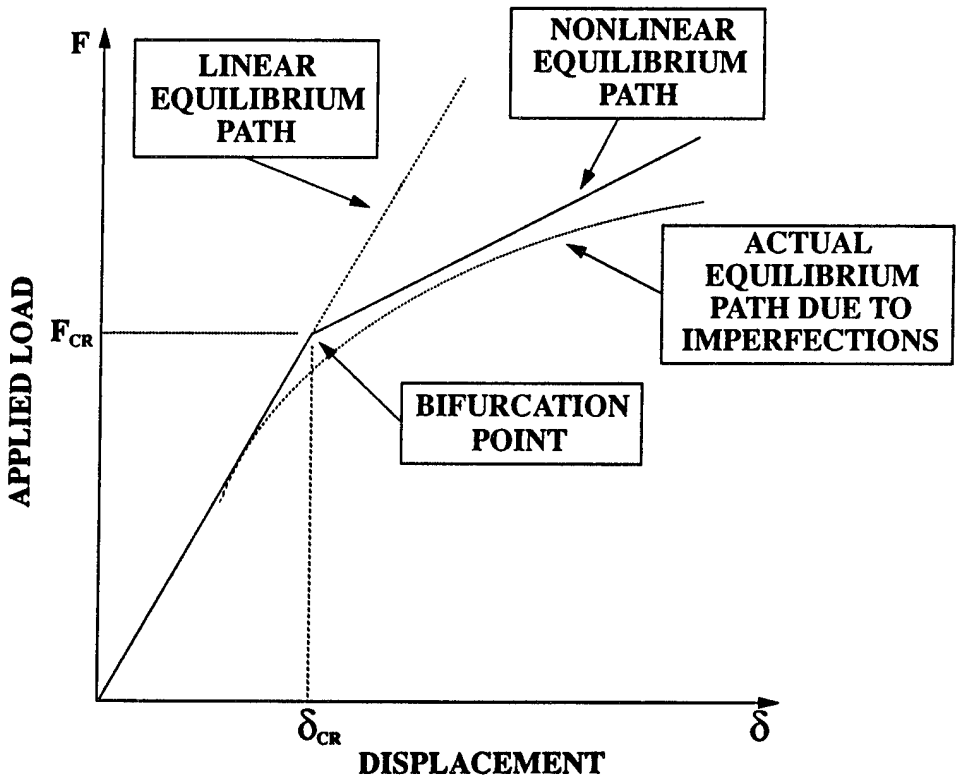

Figure 18. Bifurcation of equilibrium states.

Buckling is, therefore, a nonlinear geometric phenomemon. In order to approximate this behavior, higher-order strain terms - usually quadratic - are used to compute the differential stiffness matrix

$\mathbf{K}_\sigma$ as discussed in Section 5.2 resulting in the nonlinear equilibrium relationship

$$(\mathbf{K} + \mathbf{K}_\sigma)\mathbf{X} = \mathbf{R} \tag{95}$$

To determine the load level at which bifurcation occurs requires the solution to the following general eigenvalue problem

$$(\mathbf{K} + \frac{1}{\lambda}\mathbf{K}_\sigma)\mathbf{X} = \mathbf{0} \tag{96}$$

where the critical buckling load is then given by

$$\mathbf{R}_{crit} = \lambda\mathbf{R} \tag{97}$$

In order to determine the lowest eigenvalues of the global system, a subspace iteration is employed [113, 114]. An initial set of iteration vectors, $\mathbf{X}_k$, are selected to span the space defined by the desired eigenvectors, Φ. Iterations are then performed to converge the eigenvectors and eigenvalues in the limit

$$\mathbf{X}_k \longrightarrow \Phi \quad as \quad k \longrightarrow \infty \tag{98}$$

The subspace mapping is defined by

$$\mathbf{K}\bar{\mathbf{X}}_{k+1} = \mathbf{K}_\sigma\mathbf{X}_k \tag{99}$$

The mapping or iteration vectors are selected in accordance with a procedure outlined in Reference [113]. The selection is specified such that the first column in $\mathbf{X}$ is taken as the diagonal in $\mathbf{K}_\alpha$ while remaining columns are assigned a unit value in the row position corresponding to $min(k_{ii}/k_{\alpha ii})$. The global elastic and differential stiffness matrices are then mapped into the subspace as

$$\bar{\mathbf{K}}_{k+1} = \bar{\mathbf{X}}_{k+1}^T\mathbf{K}\bar{\mathbf{X}}_{k+1} \tag{100}$$

$$\bar{\mathbf{K}}_{\sigma k+1} = \bar{\mathbf{X}}_{k+1}^T\mathbf{K}_\sigma\bar{\mathbf{X}}_{k+1} \tag{101}$$

resulting in the reduced eigenvalue problem given by

$$\mathbf{K}_{k+1}\mathbf{Q}_{k+1} = \mathbf{K}_\sigma\mathbf{Q}_{k+1}\Lambda_{k+1} \tag{102}$$

where Λ is a diagonal matrix of the system eigenvalues. Since the initial iteration vectors are usually approximate, an improvement to the system eigenvectors is given by

$$\mathbf{X}_{k+1} = \bar{\mathbf{X}}_{k+1}\mathbf{Q}_{k+1} \tag{103}$$

and an iteration of the subspace is continued until the eigenvalues reach a stationary value defined by a tolerance as

$$\frac{|\lambda_i^{k+1} - \lambda_i^k|}{|\lambda_i^{k+1}|} \leq tol \quad , \quad i = 1,2,3,...,n \tag{104}$$

During iterations a check may be made to ensure that the smallest eigenvalues are being obtained by using the Sturm sequence property of the characteristic polynomials of eigensystems. If a shift, μ, is introduced slightly greater than the current estimate of λ_n, the factorization

$$\mathbf{K}_s = \mathbf{K} - \mu\mathbf{K}_\sigma = \mathbf{L}\mathbf{D}\mathbf{L}^T \tag{105}$$

yields a diagonal matrix, $\mathbf{D}$, in which the number of negative diagonals is equal to the number of eigenvalues smaller than μ.

An important consideration in modeling impact damaged composites is the presence of multiple delaminations schematically depicted in Figure 19.

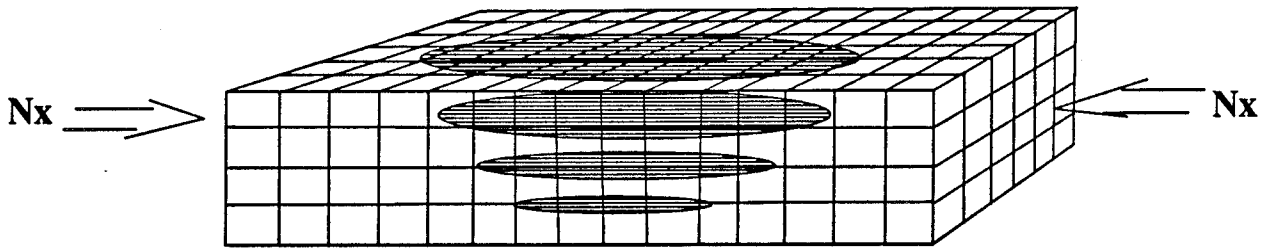

Figure 19. Laminate with multiple embedded delaminations.

The stability analysis of multiply delaminated laminates is complicated by the existence of a number of potential instability modes. If delaminations are simply modeled as planes of element discontinuity and a linear buckling analysis as detailed above is applied, predicted buckling modes will include physical modes and nonphysical modes in which the displacement of interior sublayers deform through surrounding laminate material. This behavior is depicted in Figure 20.

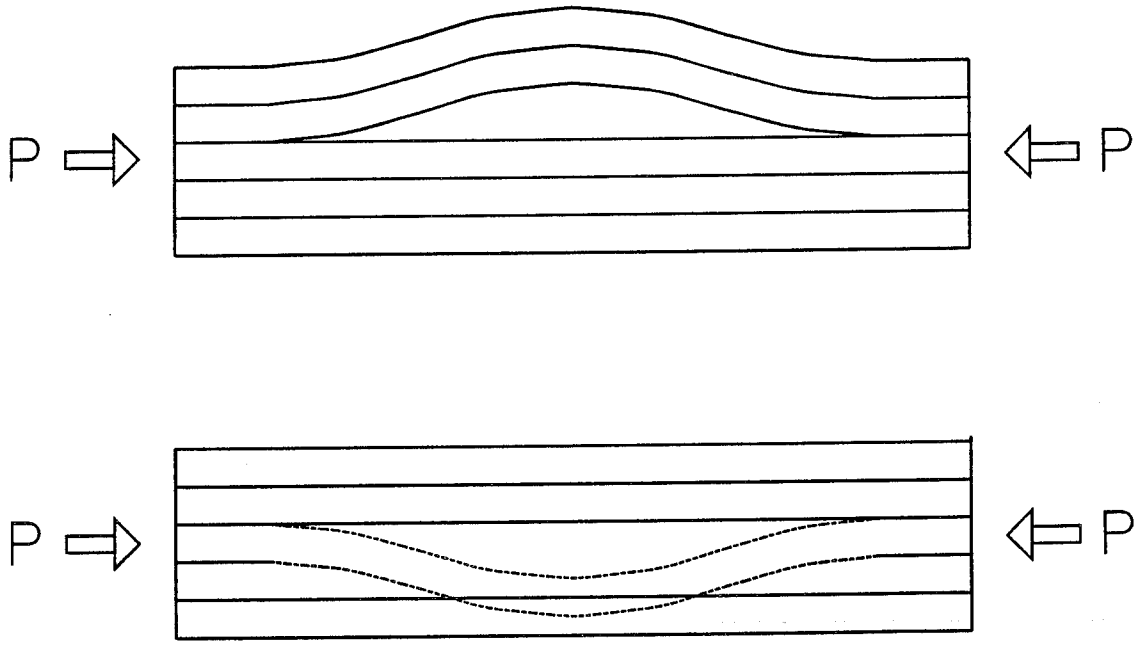

Figure 20. Physical and nonphysical sublaminate buckling modes.

The investigation of buckling in laminates containing multiple delaminations has not been adequetely addressed in the literature. Reference [12] considers a finite element study of symmetrically located delaminations and uses the crack-closure technique to suppress nonphysical or inadmissable modes. It is noted therein that when one delamination is undergoing buckling, the presence of an additional delamination represented as a plane of frictionless contact has only a slight effect on predicted buckling loads over those predicted with the second delamination removed from the model. The buckling and growth of multiple delaminations is studied in References [117, 118] using Von Karman plate theory in a finite element context to model the sublayers. An iterative scheme using the conjugate gradient method is utilized to determine equivalent contact pressures to avoid nonphysical buckling modes. Additional work on the imposition of contact constraints in finite element buckling analysis may be found in References [119, 120]. The analytical approaches demonstrate the importance of sublayer contact in the calculation of strain energy release rates and may provide a basis for further development to accurately model multiple delaminations in composites.

Combined Analysis for Residual Strength Prediction

The combined effects of accumulated material damage, inherent material nonlinearity, and potential delamination growth and sublaminate buckling significantly complicates a residual strength analysis. The material nonlinearity together with a stability analysis requires a piece–wise linear approach in which applied loads are incremented and eigenvalues extracted with buckling predicted when the largest eigenvalue is unity. In performing such a procedure, each iteration requires subiterations to converge the prediction of ply failures and delamination growth because each alters the local stiffness distribution in the laminate thereby upsetting equilibrium and internal load distribution. A schematic of the complete solution procedure is depicted in Figure 21.

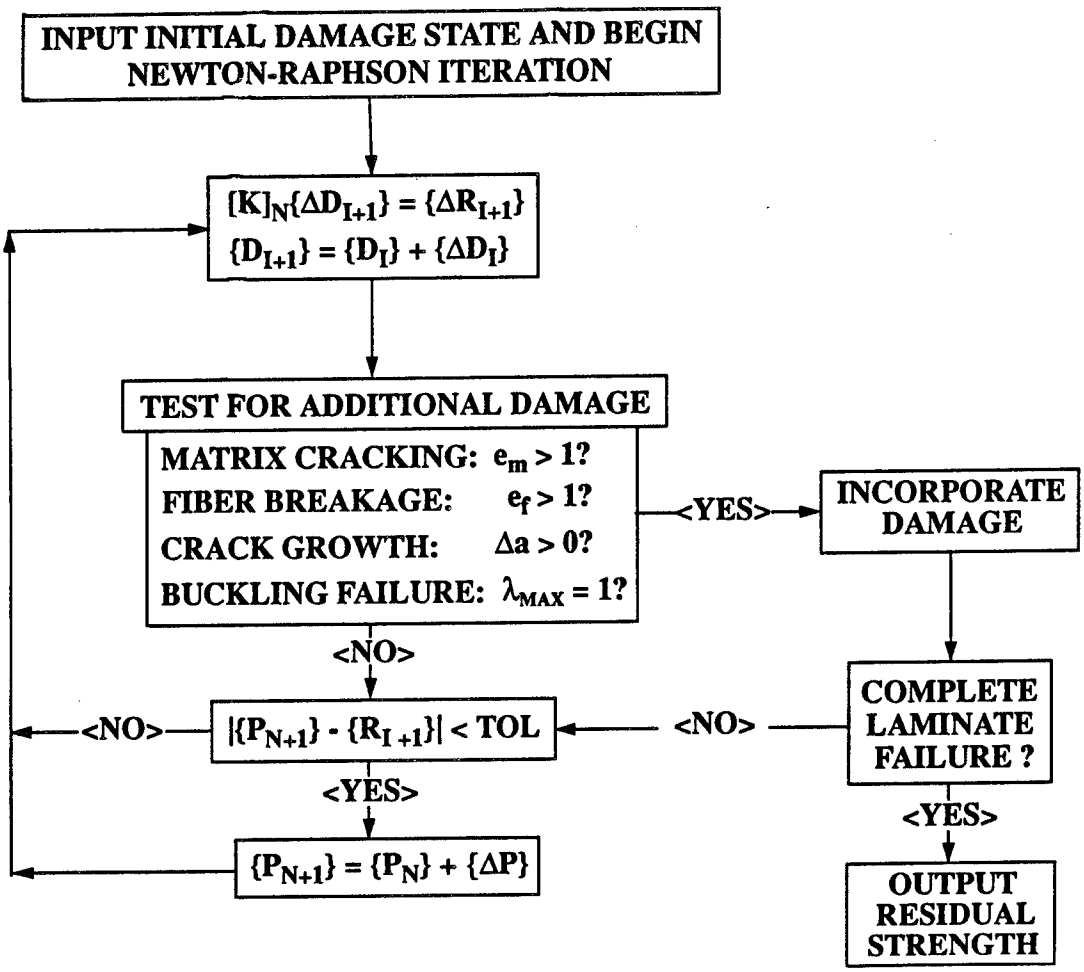

Figure 21. Flow chart of combined iterative solution algorithm.

Closure

Various modeling considerations in the prediction of residual strength in built-up composite laminates have been discussed. Regardless of the inherent accuracy of analytic modeling, the prediction of residual strength is strongly dependent on the accuracy of the inputed initial damage state. The three–dimensional state of damage may be obtained through various NDE technologies, such as Acoustic/Ultrasonics, Thermography and Radiography, each yielding different degrees of resolution in the detection of various internal damage modes.

The mathematical representation of composites must deal with three scale regimes: The microscopic, the ply and the composite component. In each regime, approximations are introduced to make the analysis tractable. At the microscopic level, the characteristics of fiber and matrix failure may be analyzed through micromechanical models to develop failure criteria and to deduce macroscopic behavior. At the ply level, the assumptions include the representation of a lamina as a homogeneous elastic continuum, the adoption of 'independent' or 'interactive' ply failure modes, degradation of elastic moduli through developed damage laws, and the approximation of nonlinear lamina behavior. At the component level, approximations are made regarding the averaging of ply material properties to develop continuous laminate elastic constants, delamination growth and sublaminate buckling behavior. Additional approximations are introduced through simplifying assumptions of component geometry, applied loading and support conditions. The variablity in the construction, properties and defects in composite components contribute to the usually wide scatter observed in experimental tests from specimen to specimen and present an inherent statistical aspect to any attempt to mathematically simulate actual composite behavior to predict residual strength.

With a consideration of the aforementioned caveats, a finite element–based numerical approach has been detailed to determine the maximum load carrying capability in damaged laminates by outlining how various laminate phenomena can be incorporated. The versatility of the finite element method in representing arbitrary geometries, boundary conditions and load conditions while accounting for material failure together with nonlinear behavior and delamination growth leading to local buckling instability should provide a more accurate representation of all relevant failure mechanisms exhibited in real laminates. These phenomena are incorporated through solution algorithms such as Newton–Raphson for material nonlinearity and subspace iteration for the prediction of buckling failure. Additional considerations such as the incorporation of large displacement and large strain effects in simulating the behavior of laminates after initial failure can be made through standard procedures existent in finite element theory.

References

[1] Madaras, E. I., Poe, C. C. and Heyman, J. S., "Combining Fracture Mechanics and Ultrasonic NDE to Predict the Strength Remaining in Thick Composites Subjected to Low-Level Impact," 1986 Ultrasonics Symposium, pp. 1051-1059.

[2] Garrett, R. A., "Effect of Manufacturing Defects and Service-Induced Damage on the Strength of Aircraft Composite Structures," *Composite Materials: Testing and Design (Seventh Conference)*, ASTM STP 893, American Society for Testing and Materials, pp. 5-33, (1986).

[3] Cairns, D. S. and Lagace, P. A., "Residual Tensile Strength of Graphite/Epoxy and Kevlar/Epoxy Laminates with Impact Damage," *Composite Materials: Testing and Design (Ninth Volume)*, ASTM STP 1059, American Society for Testing and Materials, pp. 48-63, (1990).

[4] Caprino, G., "Residual Strength Predictions of Impacted CFRP Laminates," *J. Comp. Mats.*, **18**, pp. 508-518, (1984).

[5] Lal, K. M., "Prediction of Residual Tensile Strength of Transversely Impacted Composite Laminates," *Research in Structural and Solid Mechanics - 1982*, NASA Conference Publication 2245, pp. 97-112.

[6] Shu, D. and Mai, Y. W., "Buckling of delaminated composites re-examined," *Comp. Sci. Tech.*, **47**, pp. 35-41, (1993).

[7] Chai, H., Babcock, C. D. and Knauss, W. G., "One Dimensional Modelling of Failure in Laminated Plates by Delamination Buckling," *Int. J. Solids Struct.*, Vol. **17**, No. **11**, pp.1069-1083, (1981).

[8] Lui, D., 'Delamination Resistance in Stitched and Unstitched Composite Plates Subjected to Impact Loading,' *J. Reinf. Plastics Compos.*, **9**, pp. 59-69, (1990).

[9] Simitses, G. J., Sallam, S. and Yin, W. L., "Effect of Delamination of Axially Loaded Homogeneous Laminated Plates," *AIAA*, Vol. **23**, No. **9**, pp. 1437-1444, (1985).

[10] Shivakumar, K. N. and Whitcomb, J. D., "Buckling of a Sublaminate in a Quasi-Isotropic Composite Laminate," *J. Comp. Mats.*, **19**, pp. 2-18, (1985).

[11] Wang, S. S., Zahlan, N. M. and Suemasu, H., "Compressive Stability of Delaminated Random Short-Fiber Composites, Part I - Modeling and Methods of Analysis," *J. Comp. Mats.*, **19**, pp. 296-316, (1985).

[12] Wang, S. S., Zahlan, N. M. and Suemasu, H., "Compressive Stability of Delaminated Random Short-Fiber Composites, Part II - Experimental and Analytical Results," *J. Comp. Mats.*, **19**, pp. 317-333, (1985).

[13] Madenci, E. and Westmann, R. A., "Local Delamination Growth in Layered Systems Under Compressive Load," *J. Appl. Mech. ASME*, **60**, pp. 895-902, (1993).

[14] Madenci, E. and Westmann, R. A., "Local Delamination Buckling in Layered Systems," *J. Appl. Mech. ASME*, **58**, pp. 157-166, (1991).

[15] Chang, F. K. and Chang, K. Y., "Post-Failure Analysis of Bolted Composite Joints in Tension or Shear-Out Mode Failure," *J. Comp. Mats.*, **Vol. 21**, pp. 809-833, (1987).

[16] Chang, F. K., Scott, R. A. and Springer, G. S., "Failure Strength of Nonlinearly Elastic Composite Laminates Containing a Pin Loaded Hole," *J. Comp. Mats.*, **18**, pp. 464-477, (1984).

[17] Chang, F. K. and Chang, K. Y., "A Progressive Damage Model for Laminated Composites Containing Stress Concentrations," *J. Comp. Mats.*, **Vol. 21**, pp. 834-855, (1987).

[18] Tian, Z. and Swanson, S. R., "Residual Tensile Strength Prediction on a Ply-by-Ply Basis for Laminates Containing Impact Damage," *J. Comp. Mats.*, **26**, pp. 1193-1206, (1992).

[19] Reddy, Y. S. and Reddy, J. N., "Three-Dimensional Finite Element Progressive Failure Analysis of Composite Laminates Under Axial Extension," *J. of Composites Technology & Research*, Vol **15**, No. **2**, pp. 73-87, (1993).

[20] Reddy, J. N., "On Refined Computational Models of Composite Materials," *Int. J. Num. Meth. Engrg.*, **27**, pp. 361-382, (1989).

[21] Tan, S. C., "A Progressive Failure Model of Composite Laminates Containing Openings," *J. Comp. Mats.* **25**, pp. 556-577, (1991).

[22] Ochoa, O. O. and Engblom, J. J., "Analysis of Progressive Failure in Composites," *Comp. Sci. Tech.*, **28**, pp. 87-102, (1987).

[23] Lee, J. D., "Three Dimensional Finite Element Analysis of Damage Accumulation in Composite Laminate," *Comp. Struct.*, Vol. **15**, No. **3**, pp. 335-350, (1982).

[24] Sun, C. T., "Failure Analysis of Laminated Composites by Using Iterative Three Dimensional Finite Element Method," *Comp. Struct.*, Vol. **33**, No. **1**, pp. 41-47, (1989).

[25] Carriveau, G. W., "Benchmarking of the State-of-the-Art in Nondestructive Testing/Evaluation for Applicability in the Composite Armored Vehicle (CAV) Advanced Technology Demonstrator (ATD) program," TARDEC TC No. 13604, Nov. 1993.

[26] Adams, R. D. and Cawley, P., "A Review of Defect Types and Nondestructive Testing Techniques for Composites and Bonded Joints," *NDT International*, Vol. **21**, No. **4**, p. 208-222, (1988).

[27] Rogovsky, A. J., "Engineering Selection of NDT Techniques and Accept/Reject Criteria for Composites," *New Direction in the Nondestructive Evaluation of Advanced Materials.*, pp. 45-52, (1988).

[28] Murri, W. J., Sermon, B. W., Andersen, R. N., Martinez, L. A. and VanderHeiden, E. J., "Defects in Thick Composites and some Methods to Locate Them," *Review of Progress in Quantitative Nondestructive Evaluation.*, **10(B)**, pp. 1583-1590, (1991).

[29] Berthelot, J. M. and Rhazi, J., "Acoustic Emission in Carbon Fibre Composites," *Comp. Sci. Tech.*, **37**, pp. 411-428, (1990).

[30] Daniel, I. M. and Wooh, S. C., "Ultrasonic Characterization of Defects and Damage in Thick Composites," *Review of Progress in Quantitative Nondestructive Evaluation.*, **9(B)**, pp. 1489-1496, (1990).

[31] Hamstad, M. A., "A Review: Acoustic Emission, a Tool for Composite Material Studies," *Exp. Mech.*, pp. 7-13, (1986).

[32] Michaels, T. E. and Davidson, B. D., "Ultrasonic Inspection Detects Hidden Damage in Composites," *Advanced Materials & Processes.*, **143(3)**, pp. 34-38, (1993).

[33] Hsu, D. K. and Margetan, F. J., "Analysis of Acousto-Ultrasonic Signal in Unidirectional Thick Composites Using the Slowness Surfaces," *J. Comp. Mats.*, **26(4)**, pp. 1050-1061, (1992).

[34] Schechter, R. S., Chaskelis, H. H., Mignogna, R. B. and Delsanto, P. P., "Real-Time Parallel Computation and Visualization of Ultrasonic Pulses in Solids," *Science*, Vol. **265**, pp. 1188-1192, (1994).

[35] Bakuckas, J. G., Prosser, W. H. and Johnson, W. S., "Monitoring Damage Growth in Titanium Matrix Composites Using Acoustic Emission," *J. Comp. Mats.*, **28**, pp. 305-316, (1994).

[36] Hobbs, C, and Temple, A., "The Inspection of Aerospace Structures Using Transient Thermography," *British Journal of NDT.*, **35(4)**, pp. 183-189, (1993).

[37] Jones, T. and Berger, H., "Thermographic Detection of Impact Damage in Graphite-Epoxy Composites," *Mater. Eval.*, **50(12)**, pp. 1446-1453, (1992).

[38] Henry, D. L., McCall, C. D. and Burns, B. P., "Nondestructive Evaluation of Composite Materials by Computed Tomography (CT)," Army Research Laboratory, ARL-MR-32, (1993).

[39] Lambrineas, P., Davis, J. R., Suendermann, B., Wells, P., Thomson, K. R., Woodward, R. L., Egglestone, G. T. and Challis, K., "X-Ray Computed Tomography Examination of Inshore Mine-Hunter Hull Composite Material," *NDT & E International*, pp. 207-213, (1991).

[40] Doering, E. R., Basart, J. P. and Bray, J. N., "Three-Dimensional Flaw Reconstruction and Dimensional Analysis Using a Real-Time X-Ray Imaging System," *NDT & E International*, Vol. **26**, No. **1**, pp. 7-17, (1993).

[41] Frock, B. G. and Martin, R. W., "Applications of Digital Image Enhancement Techniques for Improved Ultrasonic Imaging of Defects in Composite Materials," *Review of Progress in Quantitative Nondestructive Evaluation.*, **6(A)**, pp. 781-789, (1986).

[42] Potet, P., Jeannin, P. and Bathias, C., "The Use of Digital Image Processing in Vibrothermographic Detection of Impact Damage in Composite Materials," *Mater. Eval.*, **45(4)**, pp. 466-470, (1987).

[43] Steiner, K. V., "Image Enhancement Techniques for Ultrasonic NDE Applications," *Composite Materials: Testing and Design (10th Volume).*, **ASTM STP 1120**, pp. 330-343, (1992).

[44] Webster, R. T., Das, P. and Werner, R., "Ultrasonic Imaging for Nondestructive Evaluation of Composite Materials with Digital Image Enhancement," *1980 Ultransonic Symposium Proc.*, **Vol. 2**, pp. 873-876, (1980).

[45] Weight, K., "An Overview on NDE Methods for Thick Composites and a Proposal for Analysis of Computed Tomography Data," U.S. Army Research Laboratory, ARL TR 516, (1994).

[46] Chou, S. C. and DeLuca, E., "Dynamic Response of S-2 Glass Reinforced Plastic Structural Armor," U.S. Army Research Laboratory, ARL-SR-5, (1993).

[47] Hughes, J. D. H., "The Carbon Fibre/Epoxy Interface - a Review," *Comp. Sci. Tech.*, Vol. **41**, pp. 13-45, (1991).

[48] Tsangarakis, N. and Taleghani, B. K., "Biaxial Flexural Testing of a Carbon Fiber Reinforced Epoxy Composite," U.S. Army Research Laboratory, ARL-TR-221, (1993).

[49] Dreumel, W. H. M. and Kamp, J. L. M., "Non Hookean Behaviour in the Fibre Direction of Carbon Fibre Composites and the Influence of Fibre Waviness on the Tensile Properties," *J. Comp. Mats.*, **11**, pp. 461-469, (1977).

[50] Hahn, H. T. and Tsai, S. W., "Nonlinear Elastic Behavior of Unidirectional Composite Laminate," *J. Comp. Mats.*, **7**, pp. 102-110, (1973).

[51] Amijima, S. and Adachi, T., "Nonlinear Stress-Strain Response of Laminated Composites," *J. Comp. Mats.*, **13**, pp. 206-218, (1979).

[52] Sims, D. F., "In-Plane Shear Strain Response of Unidirectional Composite Materials," *J. Comp. Mats.*, **7**, pp. 124-130, (1973).

[53] Hashin, Z., "Failure Criteria for Unidirectional Fiber Composites," *J. Appl. Mech.*, **47**, pp. 329-334, (1980).

[54] Collins, J. A., *Failure of Materials in Mechanical Design*, John Wiley & Sons, (1981).

[55] Hill, R., 'A Theory of Yielding and Plastic Flow of Anisotropic Metals," Proceedings of the Royal Society, Series A, **193**, p. 281, (1948).

[56] Tsai, S. W., "Strength Characterization of Composite Materials," NASA CR-224, (1965).

[57] Hoffman, O., "The Brittle Strength of Orthotropic Materials," *J. Comp. Mats.*, **1**, p. 200, (1967).

[58] Tsai, S. W. and Wu, E. M., "A General Theory of Strength for Anisotropic Materials," *J. Comp. Mats.*, **5**, p. 58, (1971).

[59] Sandhu, R. S., "A Survey of Failure Theories of Isotropic and Anisotropic Materials," *Technical Report*, AFFDL-TR-72-71.

[60] Tsai, S. W., "A Survey of Macroscopic Failure Criteria for Composite Materials," *Technical Report*, AFWAL-TR-84-4025.

[61] Reddy, N. J. and Pandey, A. K., "A First-Ply Failure Analysis of Composite Laminates," *Comp. Struct.*, Vol. **25**, No. **3**, pp. 371-393, (1987).

[62] Narayanaswami, R., "Evaluation of the Tensor Plynomial and Hoffman Strength Theories for Composite Materials,", *J. Comp. Mats.*, **11**, pp. 366-377, (1977).

[63] Wu, R. Y. and Stachursky, Z., "Evaluation of the Normal Stress Interaction Parameter in the Tensor Polynomial Strength Theory for Anisotropic Materials," *J. Comp. Mats.*, **18**, pp. 456-463, (1984).

[64] Wu, R. Y, and Stachursky, Z., "Evaluation of the Normal Stress Interaction Parameter in the Tensor Polynomial Strength Theory for Anisotropic Materials," *J. Comp. Mats.*, **18**, pp. 456-463, (1984).

[65] Chang, F. K. and Lessard, L. B., "Damage Tolerance of Laminated Composites Containing an Open Hole and Subjected to Compressive Loading: Part I - Analysis," *J. Comp. Mats.*,**25**, pp. 2-43, (1991).

[66] Choi, H. Y., Wu, H. T. and Chang, F., "A New Approach Toward Understanding Damage Mechanisms and Mechanics of Laminated Composites Due to Low Velocity impact: Part II - Analysis," *J. Comp. Mats.*, **Vol. 25**, pp. 1012-1038, (1991).

[67] Lagoudas, D. C., and Saleh, A. M., "Compressive Failure Due to Kinking of Fibrous Composites", *J. Comp. Mats.*, **27**. pp. 83-106, (1993).

[68] Budiansky, B., "Micromechanics", *Comp. Struct.*, Vol. **16**, No. **1-4**, pp. 3-12, (1983).

[69] Gao, Z. and Reifsnider, K. L., "Tensile Failure of Composites: Influence of Interface and Matrix Yielding," *J. Comp. Tech. Res.*, Vol. **14**, No. **4**, pp. 201-210, (1992).

[70] Chang, F. K. and Chen, M., "The *In Situ* Ply Shear Strength Distribution in Graphite/Epoxy Laminated Composites," *J. Comp. Mats.*, **21**, pp. 708-732, (1987).

[71] Yamada, S. E. and Sun, C. T., "Analysis of Laminate Strength and its Distribution," *J. Comp. Mats.*, **12**, pp. 275-284, (1978).

[72] Chang, F. K., Scott, R. A. and Springer, G. S., "The Effect of Laminate Configuration on Characteristic Lengths and Rail Shear Strength," *J. Comp. Mats.*, **18**, pp. 290-296, (1984).

[73] Flaggs, D. L. and Kural, M. H., "Experimental Determination of *In Situ* Transverse Lamina Strength in Graphite/Epoxy Laminate," *J. Comp. Mats.*, **16**, pp. 103-116, (1982).

[74] Peter, P. W. M., "The Strength Distribution of 90° Plies in 0/90/0 Graphite Epoxy Laminates," *J. Comp. Mats.*, **18**, pp. 545-556, (1984).

[75] Garrett, K. W. and Bailey, J. E., "Multiple Transverse Fracture in 90° Cross–Ply Laminates of a Glass Fibre-Reinforced Polyester," *J. Mater. Sci.*, pp. 157-168, (1977).

[76] Talreja, R., "Transverse Cracking and Stiffness Reduction in Composite Laminates," *J. Comp. Mats.*, **19**, pp. 355-375, 1985.

[77] Highsmith, A. L. and Reifsnider, K. L., "Stiffness-Reduction Mechanisms in Composite Laminates," in *Damage in Composite Materials*, ASTM STP 775, American Society for Testing and Materials, Philadelphia, PA, pp. 103-117, (1982).

[78] Kistner, M. D., Whitney, J. M. and Browning, C. E., "First Ply Failure of Graphite/Epoxy Laminates," Poc. U.S.-Japan Conference on Composite Materials, NASA-Langley, Hampton, Virginia, (June 1983).

[79] Doucet, A. B. and Qin, J., "Microstructural Analysis of Impact Damage in Two Glass/Epoxy Composite Laminates," *Comp. Engrg.*, **3**, pp. 55-68, (1993).

[80] Rosen, B. W., "Mechanics of Composite Strengthening," *Fiber Composite Materials*, Chapter 3, American Society for Metals, (1965).

[81] Tsai, S. W. and Hahn, H. T., *Introduction to Composite Materials*, Lancaster PA: Technomic Publishing Company, (1980).

[82] Rosen, B. W., "Tensile Failure of Fibrous Composites," *AIAA*, **11**, pp. 1985-1991, (1964).

[83] Nuismer, R. J. and Tan, S. C., "Constitutive Relations of a Cracked Composite Lamina," *J. Comp. Mats.*, **22**, pp. 306-321, (1988).

[84] Pyrz, R., "A Micromechanically–Based Model for Composite Materials with Matrix Cracks," *Comp. Engrg.*, Vol. **2**, No. **8**, pp. 619-629, (1992).

[85] Jones, R. M., *Mechanics of Composite Materials*, McGRAW–HILL, (1975).

[86] O'Brien, T. K., "Characterization of Delamination Onset and Growth in a Composite Laminate," *Damage in Composite Materials, ASTM STP 775*, American Society for Testing and Materials, pp. 140-167, (1982).

[87] Kim, R. Y. and Soni, S. R., "Experimental and Analytical Studies on the Onset of Delamination in Laminated Composites," *J. Comp. Mats.*, **18**, pp. 70-80, (1984).

[88] Kim, R. Y. and Soni, S. R., "Failure of Composite Laminates due to Combined Interlaminar Shear," *Composites '86: Recent Advances in Japan and the United States*, pp. 341-350, (1986).

[89] Brewer, J. C. and Lagace, P. A., "Quadratic Stress Criterion for Initiation of Delamination," *J. Comp. Mats.*, **22**, pp. 1141-1155, (1988).

[90] Lui, D., "Impact-Induced Delaminations - A View of Bending Stiffness Mismatching," *J. Comp. Mats.*, **24**, pp. 674-692, (1988).

[91] Nairn, J. A., Lui, S. and Chen, H., "Longitudinal Splitting in Epoxy and K-Polymer Composites: Shear Lag Analysis Including the Effect of Fiber Bridging," *J. Comp. Mats.*, **25**, pp. 1086-1107, (1991).

[92] Dym, C. L. and Shames, I. H., *Solid Mechanics–A Variational Approach*, McGraw Hill, New York, (1973).

[93] Rybicki, E. F,. Schmueser, D. W. and Fox, J., "An Energy Release Rate Approach for Stable Crack Growth in the Free-Edge Delamination Problem," *J. Comp. Mats.*, **11**, pp. 470-487, (1977).

[94] Wang, S. S., "Fracture Mechanics for Delamination Problems in Composite Materials," *J. Comp. Mats.*, **17**, pp. 210-223, (1983).

[95] Rybicki, E. F. and Kanninen, M. F., "A Finite Element Calculation of Stress Intensity Factors by a Modified Crack Closure Integral," *Engrg. Fract. Mech.*, Vol. **9**, No. **4**, pp. 931-938, (1977).

[96] Irwin, G. R., *Handbuch der Physik*, **6**, p. 551, (1958).

[97] O. C. Zienkiewicz and R. L. Taylor, *The Finite Element Method*, Vol. **I**, *Basic Introduction and Linear Problem*, 4th edn. McGraw-Hill (1989).

[98] Mindlin, R. D., "Influence of Rotary Inertia and Shear on Flexural Motions of Isotropic, Elastic Plates," *J. Appl. Mech. ASME*, **18**, pp. 31-38, (1951).

[99] Lo, K. H., Christiansen, R. M. and Wu, E. M., "A Higher–Order theory of Plate Deformation, Part 1: Homogeneous Plates and Part 2: Laminated Plates," *J. Appl. Mech. ASME*, **44**, pp. 663-676, (1977).

[100] Reissner, E., "Reflections on the Theory of Elastic Plates," *Appl. Mech. Rev.*, **38**, pp. 1453-1464, (1985).

[101] Reddy, J. N., "On Refined Computational Models of Composite Laminates," *Int. J. Numer. Meth. Engr.*, **27**, pp. 361-382, (1989).

[102] Noor, A. K. and Burton, W. S., "Assessment of Shear Deformable Theories for Multilayered Composite Plates," *Appl. Mech. Rev.*, **42**, pp. 1-12, (1989).

[103] Tessler, A. and Saether, E., "A Computationally Viable Higher–Order Theory for Laminated Composite Plates," *Int. J. Num. Meth. Engr.*, **31**, pp. 1069-1086, (1991).

[104] Sciuva, M. D., "Bending, Vibration and Buckling of Simply Supported Thick Multilayered Orthotropic Plates: An Evaluation of a New Displacement Model," *J. Sound and Vibration*, **105**, pp. 425-442, (1986).

[105] Robbins, D. H. and Reddy, N. J., "Modelling of Thick Composites Using a Layerwise Laminate Theory," *Int. J. Numer. Meth. Engr.*, **36**, pp. 655-677, (1993).

[106] T. H. H. Pian and P. Tong, "Basis of Finite Element Methods for Solid Continua," *Int. J. Num. Meth. Engrg.* **1**, pp. 3-28, (1969).

[107] T. H. H. Pian and D. P. Chen, "Alternative Ways for Formulation of Hybrid Stress Elements," *Int. J. Num. Meth. Engrg.* **18**, pp. 1679-1684, (1982).

[108] T. H. H. Pian and D. P. Chen, "On the Suppression of Zero Energy Deformation Modes," *Int. J. Num. Meth. Engrg.* **19**, pp. 1741-1752 (1983).

[109] T. H. H. Pian and K. Sumihara, "Rational Approach for Assumed Stress Finite Element," *Int. J. Num. Meth. Engrg.* **20**, pp. 1685-1695, (1984).

[110] T. H. H. Pian and P. Tong, "Relations Between Incompatible Displacement Model and Hybrid Stress Model," *Int. J. Num. Meth. Engrg.* **22**, pp. 173-181, (1986).

[111] K. Y. Sze and C. L. Chow, "Efficient Hybrid/Mixed Elements Using Admissible Matrix Formulation," *Comp. Meth. Applied Mech. and Engrg.*, **99**, pp. 1-26 (1992).

[112] K. Y. Sze, "Efficient Formulation of Robust Hybrid Elements Using Orthogonal Stress/Strain Interpolants and Admissible Matrix Formulation," *Int. J. Num. Meth. Engrg.* **35**, pp. 1-20, (1992).

[113] Bathe, K. J., *Finite Element Procedures in Engineering Analysis,* Prentice-Hall, (1982).

[114] C. Lanczos, *Applied Analysis,* Dover Publications, (1988).

[115] Cook, R. D, *Concepts and Applications of Finite Element Analysis, 2nd Edition*, John Wiley & Sons, (1981).

[116] Press, W. H., Teukolsky, S. A., Vetterlin, W. T. and Flannery, B. P., *Numerical Recipes, 2nd Edition*, Cambridge University Press, (1992).

[117] Larsson, P. L., "On Multiple Delamination Buckling and Growth in Composite Plates," *Int. J. Solids Structures*, Vol. **27**, No. **13**, pp. 1623-1637, (1991).

[118] Starakers, B. and Andersson, B., "Nonlinear Plate Theory Applied to Delamination in Composites," *J. Mech. Phys. Solids*, **36**, pp. 689-718, (1988).

[119] Jeusette, J. P. and Sonzogni, V., "A Projected Conjugate Gradient Method for Structural Stability Analysis with Linear Constraints," *Comp. Struct.*, Vol. **33**, No. **1**, pp. 31-39, (1989).

[120] Whitcomb, J. D., "Analysis of a Laminate with a Postbuckled Embedded Delamination, Including Contact Effects," *J. Comp. Mats.*, **26**, pp. 1523-1535, (1992).

DISTRIBUTION LIST

No. of Copies	To
1	Office of the Under Secretary of Defense for Research and Engineering, The Pentagon, Washington, DC 20301
	Director, U.S. Army Research Laboratory, 2800 Powder Mill Road, Adelphi, MD 20783-1197
1	ATTN: AMSRL-OP-SD-TP, Technical Publishing Branch
1	AMSRL-OP-SD-TA, Records Management
1	AMSRL-OP-SD-TL, Technical Library
	Commander, Defense Technical Information Center, Cameron Station, Building 5, 5010 Duke Street, Alexandria, VA 23304-6145
2	ATTN: DTIC-FDAC
1	MIA/CINDAS, Purdue University, 2595 Yeager Road, West Lafayette, IN 47905
	Commander, Army Research Office, P.O. Box 12211, Research Triangle Park, NC 27709-2211
1	ATTN: Information Processing Office
	Commander, U.S. Army Materiel Command, 5001 Eisenhower Avenue, Alexandria, VA 22333
1	ATTN: AMCSCI
	Commander, U.S. Army Materiel Systems Analysis Activity, Aberdeen Proving Ground, MD 21005
1	ATTN: AMXSY-MP, H. Cohen
	Commander, U.S. Army Missile Command, Redstone Arsenal, AL 35809
1	ATTN: AMSMI-RD-CS-R/Doc
	Commander, U.S. Army Armament, Munitions and Chemical Command, Dover, NJ 07801
1	ATTN: Technical Library
	Commander, U.S. Army Natick Research, Development and Engineering Center Natick, MA 01760-5010
1	ATTN: SATNC-MI, Technical Library
	Commander, U.S. Army Satellite Communications Agency, Fort Monmouth, NJ 07703
1	ATTN: Technical Document Center
	Commander, U.S. Army Tank-Automotive Command, Warren, MI 48397-5000
1	ATTN: AMSTA-ZSK
1	AMSTA-TSL, Technical Library
	President, Airborne, Electronics and Special Warfare Board, Fort Bragg, NC 28307
1	ATTN: Library
	Director, U.S. Army Research Laboratory, Weapons Technology, Aberdeen Proving Ground, MD 21005-5066
1	ATTN: AMSRL-WT

No. of Copies	To
	Commander, Dugway Proving Ground, UT 84022
1	ATTN: Technical Library, Technical Information Division
	Commander, U.S. Army Research Laboratory, 2800 Powder Mill Road, Adelphi, MD 20783
1	ATTN: AMSRL-SS
	Director, Benet Weapons Laboratory, LCWSL, USA AMCCOM, Watervliet, NY 12189
1	ATTN: AMSMC-LCB-TL
1	AMSMC-LCB-R
1	AMSMC-LCB-RM
1	AMSMC-LCB-RP
	Commander, U.S. Army Foreign Science and Technology Center, 220 7th Street, N.E., Charlottesville, VA 22901-5396
3	ATTN: AIFRTC, Applied Technologies Branch, Gerald Schlesinger
	Commander, U.S. Army Aeromedical Research Unit, P.O. Box 577, Fort Rucker, AL 36360
1	ATTN: Technical Library
	U.S. Army Aviation Training Library, Fort Rucker, AL 36360
1	ATTN: Building 5906-5907
	Commander, U.S. Army Agency for Aviation Safety, Fort Rucker, AL 3636
1	ATTN: Technical Library
	Commander, Clarke Engineer School Library, 3202 Nebraska Ave., N., Fort Leonard Wood, MO 65473-5000
1	ATTN: Library
	Commander, U.S. Army Engineer Waterways Experiment Station, P.O. Box 631, Vicksburg, MS 39180
1	ATTN: Research Center Library
	Commandant, U.S. Army Quartermaster School, Fort Lee, VA 23801
1	ATTN: Quartermaster School Library
	Naval Research Laboratory, Washington, DC 20375
1	ATTN: Code 6384
	Chief of Naval Research, Arlington, VA 22217
1	ATTN: Code 471
	Commander, U.S. Air Force Wright Research and Development Center, Wright-Patterson Air Force Base, OH 45433-6523
1	ATTN: WRDC/MLLP, M. Forney, Jr.
1	WRDC/MLBC, Mr. Stanley Schulman
	U.S. Department of Commerce, National Institute of Standards and Technology, Gaithersburg, MD 20899
1	ATTN: Stephen M Hsu, Chief, Ceramics Division, Institute for Materials Science and Engineering

No. of Copies	To
1	Committee on Marine Structures, Marine Board, National Research Council, 2101 Constitution Avenue, N.W., Washington, DC 20418
1	Materials Sciences Corporation, Suite 250, 500 Office Center Drive, Fort Washington, PA 19034
1	Charles Stark Draper Laboratory, 555 Technology Square, Cambridge, MA 02139
	General Dynamics, Convair Aerospace Division, P.O. Box 748, Fort Worth, TX 76101
1	ATTN: Mfg. Engineering Technical Library
	Plastics Technical Evaluation Center, PLASTEC, ARDEC, Bldg. 355N, Picatinny Arsenal, NJ 07806-5000
1	ATTN: Harry Pebly
1	Department of the Army, Aerostructures Directorate, MS-266, U.S. Army Aviation R&T Activity - AVSCOM, Langley Research Center, Hampton, VA 23665-5225
1	NASA - Langley Research Center, Hampton, VA 23665-5255
	U.S. Army Vehicle Propulsion Directorate, NASA Lewis Research Center, 2100 Brookpark Road, Cleveland, OH 44135-3191
1	ATTN: AMSRL-VP
	Director, Defense Intelligence Agency, Washington, DC 20340-6053
1	ATTN: ODT-5A, Mr. Frank Jaeger
	U.S. Army Communications and Electronics Command, Fort Monmouth, NJ 07703
1	ATTN: Technical Library
	U.S. Army Research Laboratory, Electronic Power Sources Directorate, Fort Monmouth, NJ 07703
1	ATTN: Technical Library
	Director, U.S. Army Research Laboratory, Watertown, MA 02172-0001
2	ATTN: AMSRL-OP-WT-IS, Technical Library
5	Author